Spatial and temporal control of norovirus protease activity is determined by polyprotein processing and intermolecular interactions within the viral replication complex.

Edward Emmott[1*¶], Alexis de Rougemont[2,3¶], Jürgen Haas[4] & Ian Goodfellow[1*]

Running Title: Regulation of norovirus protease activity during infection

1. Division of Virology, Department of Pathology, University of Cambridge, Addenbrookes Hospital, Hills Road, Cambridge, UK
2. National Reference Centre for Gastroenteritis Viruses, Labology of Biology and Pathology, University Hospital Dijon Bourgogne, Dijon, France
3. AgroSup Dijon, PAM UMR A 02.102 Bourgogne Franche-Comte University, Dijon, France.
4. Division of Infection and Pathway Medicine, University of Edinburgh Medical School, Edinburgh, UK

***Corresponding author**

*Dr. Edward Emmott, ee273@cam.ac.uk

*Prof. Ian Goodfellow, ig299@cam.ac.uk

¶ These authors contributed equally.

Abstract

Norovirus infections are a major cause of acute viral gastroenteritis and a significant burden to human health globally. A vital process for norovirus replication is the processing of the nonstructural polyprotein, by an internal protease, into the necessary viral components required to form the viral replication complex. This cleavage occurs at different rates resulting in the accumulation of stable precursor forms. In this report, we characterized how precursor forms of the norovirus protease accumulate during infection. Using stable forms of the protease precursors we demonstrated that these are all proteolytically active *in vitro*, but that when expressed in cells, activity is determined by both substrate and protease localization. Whilst all precursors could cleave a replication complex-associated substrate, only a subset of precursors lacking NS4 were capable of efficiently cleaving a cytoplasmic substrate. For the first time, the full range of protein-protein interactions between murine and human norovirus proteins were mapped by LUMIER assay, with conserved interactions between replication complex members, modifying the localization of a subset of precursors. Finally, we demonstrate that re-targeting of a poorly cleaved artificial cytoplasmic substrate to the replication complex is sufficient to permit efficient cleavage in the context of norovirus infection. This offers a model for how norovirus can regulate the timing of substrate cleavage throughout the replication cycle. The norovirus protease represents a key target in the search for effective antiviral treatments for norovirus infection. An improved understanding of protease function and regulation, as well as identification of interactions between the other non-structural proteins, offers new avenues for antiviral drug design.

Introduction

Noroviruses are the causative agent of winter vomiting disease, and following the introduction of the rotavirus vaccine, a leading cause of viral gastroenteritis worldwide. Whilst models for human norovirus infection have recently been developed (1, 2), due to the availability of efficient cell culture and robust reverse genetics systems, murine norovirus (MNV) has been widely used to dissect the molecular details of viral translation and replication (3–5).

Noroviruses are small, non-enveloped positive sense RNA viruses (+ssRNA) forming a genus within the *Caliciviridae* family. As observed with many other +ssRNA viruses, noroviruses generate the majority of the viral replicase components by cleavage of a long polyprotein by the viral protease NS6 (Figure 1A) (6). A key benefit of this strategy is that due to differing rates of cleavage, polyprotein processing generates both the fully processed products and a range of stable precursor intermediates (6, 7). The role of polyprotein precursors in viral replication have been studied extensively for the *Picornaviridae* which share similarities in their polyprotein organisation (8). For noroviruses however, the sole precursor to be examined to date in any detail is the NS6-NS7 precursor (also known as Pro-Pol, or 3CD) (9, 10). Cleavage of the NS6-7 junction is known to be essential for norovirus viability and the NS6-NS7 precursor retains both protease and polymerase activities (9, 10). In contrast, for some members of the *Caliciviridae*, whilst a cleavage site between NS6 and NS7 is present, this precursor remains uncleaved (11).

Precursor protein functions are often distinct from those of the fully cleaved mature products (12). The rate of precursor cleavage and accumulation can also regulate key stages of the viral replication cycle; for example the cleavage of alphavirus non-structural proteins from the P123 and P1234 polyproteins provides temporal regulation of sense and anti-sense RNA transcript synthesis (13). In addition to cleaving viral substrates, viral proteases also target cellular proteins. We recently identified the host protein poly(A) binding protein (PABP) as a target of the norovirus protease, particularly at late stages in the viral life cycle. The cleavage of PABP forms part of a viral strategy to inhibit host translation, and therefore the production of interferon-stimulated genes (14). However the means by which PABP cleavage was restricted to late times post-infection was unclear.

Processing of the norovirus polyprotein by NS6 results in the production of six proteins; NS1/2, NS3, NS4, NS5, NS6 and NS7 (15) (Figure 1). NS5 functions as both a protein primer for RNA synthesis, as well as permitting translation of the viral genome through interactions with the host translation initiation complex (16, 17). NS6 (also known as Pro, 3C-like) and NS7 (3DPol, RdRP) encode the 3C-like protease and RNA-dependent RNA polymerase respectively. The N-terminal 3 proteins are less well characterized but are known to localize to cytoplasmic membranes. NS1/2 localises to the endoplasmic reticulum (18), and is implicated in viral persistence (19). NS3 has NTPase (20) and predicted RNA helicase activities, and was recently shown to interact with cholesterol-rich

membranes and cytoskeletal proteins (21). NS4, an orthologue of the picornavirus 3A protein, is localized to endosomes (18).

In this study we identify a mechanism by which noroviruses regulate viral protease cleavage of substrates during the viral replication cycle. We demonstrate how polyprotein processing controls protease localization and as a result, substrate accessibility, providing a mechanism for temporal regulation of protease cleavage of substrates. Furthermore, we have demonstrated that a comprehensive network of protein-protein interactions occur between the viral replicase proteins which also regulates protease and precursor localization. Finally we demonstrate that targeting an artificial substrate to the viral replication complex allows cleavage by authentic viral protease produced during infection. As the polyprotein includes key drug targets including the protease and polymerase (22, 23), an improved understanding of how these proteins function and are regulated throughout the viral life cycle may aid drug design and targeting.

Results

The norovirus protease cleaves a cytoplasmic FRET substrate upon transfection but not in the context of infection

We sought to examine whether norovirus protease precursors play an important role in regulating substrate cleavage. To this aim, we compared the ability of the NS6 protease to cleave an artificial substrate when produced either as a fully processed form or produced during authentic viral replication. We have previously reported the generation of a FRET sensor for assessing norovirus

124 protease activity in live cells (7). This FRET sensor consists of CFP fused to YFP
125 via a short linker region consisting of the P7 to P7' region of the MNV NS1/2-3
126 cleavage site (Figure 1B). Whilst the expression of the mature protease resulted
127 in efficient cleavage of the sensor, recapitulating our previous results, protease
128 produced during viral infection showed extremely poor cleavage of the FRET
129 sensor (Figure 1C). Western blotting for NS6 protein confirmed the presence of
130 higher molecular weight isoforms of NS6 during infection (Figure 1C). These
131 higher molecular weight proteins likely represent precursor forms of the
132 protease, that we and others have observed previously (6, 7).
133
134 To examine whether poor cleavage of the FRET substrate during infection was
135 due to a mismatch between substrate and protease localization, the localization
136 of the protease and sensor was examined following transfection or infection of
137 HeLa cells expressing the recently identified MNV receptor CD300lf (24, 25).
138 Confocal microscopy revealed that the FRET sensor displayed diffuse nuclear
139 and cytoplasmic localization, in both transfected and infected cells (Figure 1D).
140 Whilst NS6 produced following transfection showed the same diffuse localization
141 as the FRET sensor, in infected cells NS6 was located primarily to a large
142 perinuclear puntca, consistent with previous observations (17) and most likely
143 reflecting the position of the viral replication complex (RC). Given that the NS6
144 antisera recognizes both mature and precursor forms of NS6, the localization
145 pattern likely represents an averaged localization for both mature NS6 and NS6-
146 containing precursors. These data suggest that substrate cleavage during
147 infection is likely impacted by precursor and substrate localisation, and that the

148 context in which NS6 is expressed may affect the relative efficiency with which a
149 substrate is cleaved.
150
151 **Targeting a cytoplasmic substrate to the replication complex permits**
152 **efficient cleavage by NS6**
153 To determine if poor substrate-protease co-localization was responsible for the
154 low levels of cleavage observed during infection we fused the FRET substrate to
155 the C-terminus of NS7 in the context of full-length polyprotein, with either a WT
156 (ORF1-FRET-WT) or a catalytically inactive protease domain (ORF1-FRET-
157 H30A), in order to drive RC localization. Polyprotein processing was unaffected
158 by fusion to the FRET sensor as the relative level of mature NS5 and NS5-
159 containing precursors was similar to those generated from a MNV full-length
160 infectious clone (MNV-FLC-WT, Figure 2A). The FRET sensor was efficiently
161 cleaved in the context of the ORF1-FRET-WT construct, producing a ~70kDa
162 NS7-CFP fusion product which was increased in mass when expressed in the
163 context of ORF1 with a catalytically inactive protease (ORF1-FRET-H30A)
164 (Figure 2A). We also observed that the fusion of the FRET sensor to ORF1
165 resulted in RC localization as the CFP signal localized to the perinuclear region
166 where the RC is known to form (Figure 2B). As expected, the RC localization of
167 the YFP component of the FRET sensor was more pronounced when expressed in
168 the context of ORF1 with a catalytically inactive protease (ORF1-FRET-H30A,
169 Figure 2B). These data confirm that targeting of an artificial protease substrate
170 to the RC allows for efficient cleavage of the substrate, adding to our hypothesis
171 that protease localization and/or the context in which the protease is expressed,
172 affects substrate cleavage efficiency.

NS6-containing precursors are abundant and expressed from early times in infection

The processing of the norovirus polyprotein at the five known cleavage sites would, in principle, result in the generation of 21 distinct protein products, of which 10 would be predicted to contain the protease domain (Table S1). To investigate precursor abundance, the presence of precursors during viral replication was examined by western blot (Figure 3). The identity of the observed precursors was assigned based on reactivity with either NS6 or NS5 antisera, predicted molecular weight, comparing migration on SDS-PAGE to a transfected stable form of the individual precursor (Figure S1), and previously published observations (6). NS6- (Figure 3A) and NS5-containing precursors (Figure 3B) were observed as early as 3-4h post-infection, although the predominant NS6 containing precursor seen throughout infection was in fact NS4-6. The majority of the other predicted NS6-containing precursors could be identified including full-length NS1/2-7 (Figure 3A and B).

Although the NS6-7 precursor was previously suggested to be the major form of NS6 contributing to norovirus polyprotein cleavage based on increased activity *in vitro* compared to mature NS6 (9), our data would indicate that it is produced at relatively low levels. Mature, fully-processed NS6 appears to be the major form of NS6 present over the course of infection. Infectious virus production occurs from 5h post-infection onwards (Figure 3C) at times when the mature form of NS6 and the NS4-6 and NS4-7 precursors are the major forms of NS6 present at detectable levels.

198

199 To examine if the localization of NS6 was influenced by the context of the
200 precursors in which it is contained, we used crude fractionation to separate cells
201 into cytoplasmic and membrane-associated fractions (Figure 3D). The
202 distribution of the soluble cytoplasmic and membrane-associated protein
203 marker proteins GAPDH and VDAC confirmed successful fractionation (27). The
204 MNV NS1/2, NS3 and NS4 proteins are known to be membrane associated (18,
205 21), and our results confirmed NS3 was restricted to the membrane fraction. NS7
206 associates with the RC, but lacks a predicted trans-membrane domain and could
207 be found in both fractions. The distribution of NS5-containing precursors was
208 used as a surrogate for NS6 due to the significant overlap with NS6-containing
209 precursors and the greater sensitivity of the antisera. High molecular weight
210 precursors containing NS1/2, NS3 or NS4, were absent from the soluble
211 cytoplasmic fraction. In particular the most abundant higher molecular weight
212 precursor (NS4-7) was exclusively isolated in the membrane fraction. Proteins
213 present in the soluble cytoplasmic fraction included fully processed NS5, a
214 protein which may represent NS4/5 or NS5/6, and NS5-7. NS4-6 was present
215 but significantly less abundant in the cytoplasmic than membrane fraction. Some
216 <15kDa proteins were identified in the membrane fraction which may represent
217 modified forms of NS5, or breakdown products. Taken together these data
218 confirm that precursor forms of the norovirus replicase proteins impart distinct
219 patterns of localization on polyprotein constituents, which can differ from their
220 fully processed forms.

221

Precursor forms of the norovirus protease are proteolytically active in a cell-free system but show variable activity in cells

As NS6-containing precursors showed variation in their localization in infected cells, we hypothesized that this would also result in variation in their ability to cleave substrates. To test this hypothesis, active, stable forms of these precursors were generated by alanine mutagenesis of the P1 residue (28) at each cleavage site. Of the 21 polyprotein products that can be generated by NS6-mediated polyprotein cleavage, ten contain NS6 (Figure 4A). All protease-containing precursors could be readily expressed *in vitro* and in transfected cells, although to varying degrees (Figure B and C). Expression in both systems yielded proteins of the expected molecular weights (Figure 4A, Table S1). We next examined the ability of each precursor to cleave two different substrates; the ORF1-FRET-H30A substrate, and poly-A-binding protein (PABP), a cellular protein involved in translation that we previously identified as being cleaved by NS6 during norovirus infection (14). When unlabeled *in vitro* translated norovirus protease-containing precursor proteins were incubated with *in vitro* translated ^{35}S-methionine labelled PABP, cleavage products were observed (Figure 4D). As expected, cleavage products were not observed upon incubation of PABP with catalytically inactive protease (H30A). It is noteworthy that only a fraction of the PABP produced *in vitro* was cleaved, fitting with our previous observations (14). However, when the protease precursors and FLAG-tagged PABP were co-expressed in cells, a C-terminal PABP cleavage product, detected by virtue of the C-terminal FLAG tag, was only observed when co-expressed with NS6, NS6-, NS5-6 and NS5-7(Figure 4E). The ability of the precursors to cleave a protease substrate that was localized to the viral replication complex was examined by co-

247 transfection of cells with plasmids expressing the precursors and the ORF1-
248 FRET-H30A FRET substrate (Figure 4F). FRET substrate cleavage was observed
249 in all cases except when co-transfected with a catalytically inactive mature
250 protease. In a limited number of cases, in addition to the fully cleaved FRET
251 substrate, additional larger CFP/YFP containing precursors were observed with
252 some protease-containing precursors that were not detected following co-
253 expression with the mature protease. Together these data highlight that the
254 context in which NS6 is expressed and the localization of any given substrate,
255 alters the relative efficiency of substrate cleavage.
256
257 **NS6 precursor localization is determined by fusion of NS6 with membrane-**
258 **bound polyprotein components and intra-replication complex interactions.**
259 To examine how the context in which NS6 is expressed affects its localization we
260 examined the localization of each precursor in HeLa cells expressing the MNV
261 receptor (CD300lf) by confocal microscopy (Figure 5). The mature fully
262 processed form of NS6 and the NS5-6 precursor showed predominantly
263 cytoplasmic localization, with some nuclear localization. The localization of the
264 other precursors was more varied. NS6-7 also showed some degree of nuclear
265 localization but was largely localized to the cytoplasm. NS5-7 was exclusively
266 localized to the cytoplasm but also formed some cytoplasmic puncta. NS4-6 and
267 NS4-7 showed reticular localization, reminiscent of RC localization. A detailed
268 analysis of the localization of the longer precursors was confounded by the
269 relatively poor expression and toxicity of these precursors following transfection
270 however a limited number of cells could be visualized by confocal microscopy
271 Figure S2. The NS3-containing precursors NS3-6 and NS3-7 localized to small,

spherical cytoplasmic membranous structures whereas the NS1/2-6 and NS1/2-7 precursors were largely cytoplasmic, with some cytoplasmic, possibly membrane associated puncta, observed on the case of NS1/2-6. In summary, we found that the precursors containing NS4 and NS3 imparted membrane localization on NS6, consistent with these proteins localizing to the viral RC. These data were also consistent with the poor efficiency with which these precursors cleave PABP (Figure 4E).

Previous studies indicate that NS7 localizes to the viral RC suggesting in the context of viral infection, suggesting that protein-protein interactions between the viral replicase proteins likely also affects polyprotein localization. To test this hypothesis we examined the impact of viral infection on the localization of each NS6 containing precursor (Figure 5). Whilst the localization of mature NS6, NS4-6 and NS4-7 was not altered upon infection, the NS5-6, NS6-7 and NS5-7 precursors were redistributed to the viral RC. In the case of NS5-6, whilst cytoplasmic and nuclear localization was still visible, there was clear enrichment at the viral RC as evident by colocalization with viral dsRNA. NS6-7 and NS5-7 showed a more pronounced relocalization following infection, with the vast majority of these precursors localized to the RC.

Identification of protein-protein interactions between norovirus proteins

The relocalization of NS7-containing precursors to the viral RC upon infection highlighted the potential role of interactions between viral components to tether NS6-containing precursors to the viral RC. We therefore examined the network of interactions between norovirus replicase proteins in order to determine

297 which of these might impact on precursor localization. To this aim we used the
298 LUMIER system (29, 30) to map all the interactions between individual MNV
299 proteins (Figure 6 and S3). A similar analysis was also performed for GI.1 and
300 GII.4 human norovirus (Figures S4 and S5) to identify conserved intra-RC
301 protein-protein interactions. Strong self-association was observed with NS1/2,
302 NS4, NS7, and the major and minor capsid proteins VP1 and VP2. The N-terminal
303 components of the polyprotein NS1/2, NS3 and NS4 interacted with each other,
304 all of which have previously been shown to localize to cytoplasmic membranes in
305 order to initiate RC formation for the related feline calicivirus (31). As expected,
306 a robust interaction between the VP1 and VP2 capsid proteins was seen along
307 with VP1-NS7 and NS1/2-NS7 interactions. These latter interactions fit with our
308 previous observations of the impact of VP1 and NS1/2 on polymerase function
309 (32). A interaction was also observed between NS5 and NS7, in keeping with the
310 role of NS5 in serving as a protein primer for RNA synthesis. These data suggest
311 that the redistribution of the NS6 containing precursors NS5-6, NS6-7 and NS5-7
312 to the viral RC is therefore the likely result of interactions between NS1/2 and
313 NS7, which in the case of NS5-6 could occur via the formation of a NS5-
314 6:NS7:NS1/2 complex.
315
316 **Fusion to N-terminal replication complex components permits effective**
317 **cleavage of fused substrates by the norovirus protease *in trans*.**
318 To examine the minimum features requires for the correct localization of a
319 substrate to the viral RC and its subsequent cleavage, a range of truncation and
320 deletion mutants in the ORF1-FRET-H30A construct were generated to
321 determine which components were necessary and sufficient for cleavage *in trans*

(Figure 7A). Active RC localized viral protease was provided *in trans* by co-expressing the FRET substrates with a MNV full length cDNA clone with either a wild-type (MNV-FLC) or catalytically inactive protease (MNV-H30A).

The N-terminal truncations all displayed some degree of cleavage with the NS7-FRET substrate being cleaved the least efficiently (Figure 7B). Whilst the fusion of NS7 alone to a substrate was sufficient to allow *trans* cleavage, C-terminal truncations demonstrated that NS7 was not essential as the NS1/2-6, NS1/2-5 and NS1/2-4 fusions were all cleaved efficiently (Figure 7C). The NS1/2-3 and NS1/2 fusions showed progressively poorer cleavage of the fused substrate, with negligible cleavage observed with the latter.

Finally, the impact of internal deletions on FRET substrate cleavage was examined (Figure 7D). The ΔNS4 mutant showed a minor defect in cleavage, which may have been due to the chimeric nature of the NS3/5 cleavage site generated by the deletion. Single deletions of NS3, NS4, NS5 and NS6 all permitted efficient cleavage. From this data it is apparent that no single region of the polyprotein was essential for cleavage of a fused substrate, but that several regions of the polyprotein (NS1/2-4 or NS7) appeared sufficient. These regions matched those identified earlier as sufficient for RC localization (Figure 6), either directly, or through interactions with other viral RC components.

Replication complex localization of FRET substrates permits cleavage by the norovirus protease in the context of infection

346 Having identified the minimal regions required for RC-targeting of fused
347 substrate by polyprotein and precursors provided *in trans*, we predicted that
348 these fusions would permit the cleavage of said substrate by MNV in the context
349 of infection. The full length ORF1-FRET-H30A fusion and three of the deletion
350 constructs (NS7, NS1/2-4, NS1/2) were chosen for further characterisation.
351
352 As anticipated, the ORF1-FRET-H30A fusion was efficiently cleaved during viral
353 infection at both 9h (Figure 8A) and 12h (Figure 8B) post-infection. NS1/2-4-
354 FRET was mostly cleaved at 9h post infection and showed full cleavage by 12h
355 post infection. This NS1/2-4 fusion represented the most efficiently cleaved of
356 the truncated substrates. The NS1/2-FRET fusion showed poor cleavage at 9h
357 post-infection (Figure 8A), consistent with our previous observations (Figure
358 7C), but cleavage was significantly increased by 12h post infection. The NS7-
359 FRET fusion remained largely uncleaved at both 9h or 12h post-infection (Figure
360 8A/B). Combined, these data highlight that substrate accessibility and protease
361 localization, may be at least one mechanism by which norovirus temporally
362 regulates the cleavage of any given substrate.
363

364 ## Discussion

365 The generation of viral replicase components from a single large polyprotein is a
366 mechanism conserved in many +ssRNA viruses including noroviruses. The
367 regulated production of viral precursors, often with distinct functions, enables
368 the expansion of functional coding capacity without a concomitant increase in
369 viral genome size.
370

371 In the case of noroviruses, 21 possible precursors can be generated by NS6
372 cleavage of the polyprotein, ten of which contain the protease. In this study we
373 confirm that all ten of these protease-containing precursors represent active
374 forms of the protease, though spatial sequestration of a number of these
375 precursor forms controls their substrate accessibility. Due to similarity with
376 other caliciviruses, where the protease and polymerase (NS6-7) remain
377 uncleaved, NS6-7 had previously been suggested to represent the dominant form
378 of NS6 proteolytic activity (33). In support of this hypothesis, NS6-7 retains both
379 proteolytic and polymerase activity whilst fused (9, 10), can more efficiently
380 nucleotidylate NS5 than NS7 alone (34), and NS6-7 has higher proteolytic
381 activity than NS6 alone *in vitro* (33). However, our data questions the extent to
382 which this precursor may contribute to these activities as we identified the NS4-
383 6 precursor as the most abundant precursor form produced over the course of
384 an infection. We also found that NS6-7 does not localize directly to the viral RC,
385 but instead requires other viral factors such as NS1/2 for this localization. In
386 addition, we have previously shown that the NS6-7 cleavage site is efficiently
387 cleaved, consistent with the extremely low levels of NS6-7 observed throughout
388 our timecourse experiments (7). Whilst abundant, the diffuse localization of
389 fully cleaved NS6 would result in lower concentrations of this form of the
390 protease both within the replication complex and throughout the cytoplasm as a
391 whole. This would prevent efficient cleavage by NS6 until very late times post-
392 infection. We would therefore hypothesise that NS4-6 represents the form of the
393 protease responsible for the majority of *trans* polyprotein cleavage observed
394 during norovirus infection. The cytoplasmic localization of mature NS6 could
395 provide a mechanism of controlling the levels of viral protein cleavage by

396 expelling excess protease from the RC, and thus avoiding runaway levels of
397 proteolysis as polyprotein abundance increases. In addition, this may allow for
398 the temporal regulation of the cleavage of certain cellular substrates. It should
399 however be noted that whilst this study primarily focuses on *trans*-cleavage by
400 the protease, cis-cleavage most likely plays an important role in norovirus
401 polyprotein processing and will require further research.
402
403 In a recent study we identified PABP as a cellular substrate of the norovirus
404 protease (14). Cleavage of PABP at late times post-infection partially accounted
405 for inhibition of host translation and diminished production of innate immune
406 regulatory proteins during MNV infection. Transfection of a non-cleavable form
407 of PABP resulted in reduced in MNV replication (14). The mechanism behind the
408 temporal regulation of PABP cleavage is unknown as mature protease is
409 produced early in infection. From the data presented here, the shorter, non-
410 membrane associated forms of NS6 more effectively cleaved PABP. PABP is a
411 cytoplasmic protein much like the unfused FRET substrate. Whilst the fully-
412 cleaved NS6 is the most abundant form of the protease for much of infection, its
413 diffuse localization would be expected to result in lower concentrations of total
414 protease in the cytoplasm, compared with the replication complex which would
415 also possess the membrane-associated protease precursors. This hypothesis is
416 consistent with the strong replication complex localization observed using anti-
417 NS6 antisera in MNV-infected cells. The concentration of NS6 activity within the
418 RC until late times post-infection may represent the means by which PABP
419 cleavage is temporally regulated, with PABP cleavage only observed once
420 cytoplasmic NS6 concentrations have reached a threshold level.

421

422 A network of interactions between viral replication complex proteins, their
423 precursor forms, and a range of cellular proteins is required to establish the
424 formation of a functional viral RC (35, 36). The interactions between the feline
425 calicivirus replicase proteins have been previously investigated by our group
426 using the yeast two-hybrid system (37). In the current study we extended this to
427 include noroviruses, identifying a network of evolutionarily conserved
428 interactions. Surprisingly, we observed no direct interactions with the mature
429 NS6 and any other viral proteins. Further studies are required to determine if
430 this is due to confounding effects of the additional sequences added for the
431 LUMIER assay. However, NS6 has the potential to interact with NS1/2, NS5 and
432 VP1 when part of the NS6-7 precursor, and NS4-6 precursors would also be
433 expected to interact with NS1/2 and NS3 through interactions with the NS4
434 component of the precursor. Several distinctions between norovirus protein-
435 protein interactions and the previous calicivirus protein interaction study were
436 observed. FCV p76 (equivalent to NS6-7) weakly interacted with the minor
437 capsid protein (37), whereas no interactions between VP2 and the non-
438 structural proteins were observed for the noroviruses. For noroviruses NS1/2
439 appears to play the key role in binding a number of the non-structural proteins
440 together by interacting with NS3, NS4 and NS7, with FCV p32 playing a similar
441 role (37). However the self interactions of NS3 and NS4 observed in the LUMIER
442 data were not conserved in their FCV p39 and P40 equivalents (37).

443

444 Cleavage of a subset of FRET fusion substrates showed some variation between
445 infection and transfection-based *trans*-cleavage studies. NS1/2 fusions, unlike

446 NS1/2-4 fusions, were poorly cleaved following co-transfection with active
447 protease, but were subsequently cleaved, albeit at very late times, in the context
448 of MNV infection. However, the superior cleavage of the NS1/2-4 fusion can be
449 understood in the context of the LUMIER data which highlights interactions
450 between NS1/2, NS3 and NS4. Both substrate and protease expression in the
451 trans-cleavage assay system is driven to high levels by T7-driven expression. In
452 particular, this would be expected to produce significantly more NS1/2-FRET in
453 this system, without a concomitant increase in the NS3 and NS4, an issue not
454 present with the NS1/2-4-FRET substrate. This aberrant stoichiometry between
455 NS1/2, NS3 and NS4 may result in not all of the NS1/2-FRET substrate
456 integrating successfully into the RC. At the lower levels of substrate expression
457 achieved following electroporation into BV-2 cells, a higher proportion of the
458 NS1/2-FRET substrate may be incorporated into the RC, albeit at late times post
459 infection resulting in the cleavage of this substrate at 12h but not 9h post-
460 infection.
461
462 The alphaviruses represent the best-characterised example of polyprotein
463 cleavage driving the staging of events in the viral life cycle throughout
464 replication (13). Compared with noroviruses, the alphaviruses have a simpler
465 polyprotein with two alternate forms P123 and P1234 produced by stopcodon
466 readthrough. The successive processing of this polyprotein at the P34, P12 and
467 P23 junctions respectively controls a shift in viral transcription from negative to
468 positive sense transcription (13). Accumulation of the protease, and control of
469 cis- and trans-cleavage activity throughout infection drives these shifts in

precursor populations and thus yields a mechanism for temporal regulation of viral replication.

Whilst our current understanding of the roles of norovirus precursor proteins and polyprotein cleavage is less developed than for the alphaviruses, the localization, interactions, and cleavage patterns of the various protease precursors gives rise to a basic mechanistic model for how polyprotein cleavage could regulate some aspects of the norovirus life cycle. Following release of the viral genome has into the cytoplasm, pioneer rounds of translation of the polyprotein from the incoming genome occur. The synthesis of viral negative sense RNA is thought to occur via a *de novo* initiation mechanism that is enhanced by an interaction between the viral capsid protein VP1 and the polymerase NS7 (38–40). The production of viral VPg-linked positive sense RNA can then occur. Analyses of NS5/VPg-linked RNA produced in norovirus infected cells have to date only found fully processed NS5 linked to RNA (16). However, experiments with the distantly-related picornaviruses showed that in cases where the NS5-6 equivalent (3BC) cleavage site was mutated, viable virus was obtained and 3BC could be identified bound to the RNA (41). This suggests that the priming functions of NS5 may not require the fully processed protein. However our group and others have confirmed that the fully processed NS5 is most efficient at binding to eukaryotic initiation factor proteins and therefore translation of viral proteins (16, 42). For example, Leen and colleagues demonstrated that the disruption of NS5-6 cleavage abolished the interaction of NS5 with the eIF4G HEAT domain (42). Regulation of the levels of NS5-containing precursors may therefore provide a mechanism of temporal

495 regulation of viral RNA synthesis, due to the progression in precursor abundance
496 from dominant NS4-6 and NS4-7 forms at early times, to later times when the
497 fully cleaved and shorter precursors (NS4-5, NS5-6) are more abundant.
498 Negative sense RNA synthesis would be anticipated to dominate until sufficient
499 NS5 is present in a suitable (presumably shorter) precursor form to permit sense
500 transcription. In addition this temporal regulation of the NS5 precursor state
501 may also control levels of translation, though how distinct the NS5 cleavage state
502 requirements for efficient translation are from those for positive sense RNA
503 synthesis remains to be fully elucidated.
504
505 In conclusion, our study identified a mechanism by which noroviruses may
506 regulate protease activity. This is achieved by both the temporal control of
507 precursor production and the spatial regulation this imparts either directly or
508 indirectly via intra-RC protein-protein interactions with other viral replicase
509 components. Membrane tethering keeps precursors associated with the RC,
510 serving to concentrate their activity and ensure efficient cleavage of viral or RC-
511 associated substrates. At late times shorter forms of the protease lacking either a
512 transmembrane fusion partner such as NS4, or the ability to interact indirectly
513 with the replication complex via NS7 dominate. These forms are no longer
514 sequestered at the RC and are capable of cleaving cytoplasmic substrates. This
515 understanding of which forms of the protease are most active throughout
516 infection, and their regulation may serve to guide future drug design efforts
517 against the protease and other RC components.
518

519 **Methods**

520 Cells and Viruses

521 Murine BV-2 cells were used for infection experiments (25); human HeLa cells
522 expressing the murine norovirus receptor (HeLa-CD300lf) and hamster BSR-T7
523 cells were used for transfection and microscopy experiments. Experiments using
524 fowlpox T7-mediated expression of the polyprotein, or polyprotein fusions from
525 the MNV reverse genetics system were performed in BSR-T7 cells as described
526 (43). LUMIER assays were performed in unmodified HEK-293T cells.

527

528 All infections were performed with murine norovirus strain CW1 (43).
529 Preparation and titration of virus stocks by $TCID_{50}$ was performed as described
530 (44). All infections were performed at high multiplicity of infection (MOI: 10
531 $TCID_{50}$/cell). Cells were cultured in DMEM media supplemented with
532 penicillin/streptomycin, 10% serum, and were maintained at 37°C, 5% CO_2. With
533 the exception of BV-2 cells, transfections were performed in antibiotic-free
534 media using Lipofectamine 2000 (Life Technologies) as per the manufacturer's
535 recommendations. BV-2 cells were electroporated with *in vitro* transcribed RNAs
536 using the Neon electroporation system (Life Technologies) as described
537 previously (45).

538

539 Plasmids and molecular cloning

540 The FRET plasmid used was essentially as described in (7). To avoid difficulties
541 in PCR amplification of the FRET sensor (CFP-cleavable linker-YFP) due to high
542 sequence identity between the CFP and YFP coding sequences, this was re-cloned
543 using a modified YFP nucleotide sequence whilst maintaining the original linker

544 and protein sequences (sequence available upon request). The generation of the
545 FLAG-PABP plasmid has been described previously (14).
546
547 N-terminally FLAG-tagged stable forms of all the potential NS6 containing
548 precursors were generated in pTriex1.1 (Novagen) using pT7 MNV 3'RZ (43) as a
549 template. In each precursor, all the known cleavage sites had their P1 residue
550 mutated to alanine to inhibit cleavage. Cloning was accomplished by Gibson
551 assembly into the NcoI and XhoI restriction sites of pTriex1.1.
552
553 The pT7 MNV 3'RZ plasmid used has been described previously (43), and
554 represents a full-length clone of the MNV CW1 strain (DQ285629), and is
555 referred to as MNV-FLC in the manuscript. The proteolytically inactive form of
556 this plasmid was generated by alanine mutagenesis of His30 within the NS6
557 sequence (MNV-H30A). The full-length FRET fusion plasmid (ORF1-FRET-WT)
558 and inactive mutant (ORF1-FRET-H30A) were derived from pT7 MNV 3'RZ and
559 had the subgenomic region deleted and the FRET sensor fused to NS7 in place of
560 the NS7 stop codon. A poly(A) tail was included between the stop codon of the
561 FRET sensor and the HDV ribozyme. This permitted expression of this protein by
562 transfection of the plasmid into BSR-T7 cells infected with fowlpox-T7, or by
563 electroporation of *in vitro* transcribed RNA into BV-2 cells.
564
565 The various deletion constructs based on ORF1-FRET-H30A were generated by a
566 Gibson assembly approach. N-terminal deletions all incorporated the methionine
567 from NS1/2. C-terminal deletions fused the FRET sensor to the C-terminal-most
568 protein which had its C-terminal P1 residue directly joining the FRET sensor

mutated to alanine to prevent off-target cleavage between the C-terminal protein and CFP. For internal deletions, the sequence deleted extended from the P1' of the N-terminal cleavage site to the P1 of the C-terminal cleavage site of the protein of interest resulting in the production of a chimeric cleavage site. For example, in the NS3 deletion mutant, the cleavage site between NS1/2 and NS4 consists of the P side residues of the NS1/2-NS3 cleavage site and the P' side residues of the NS3-NS4 cleavage site.

All MNV and genogroup I and II HuNoV genes encoding individual proteins were cloned from MNV-1 (strain CW1) and Norwalk (GI.1) into the Gateway® pDONR207 entry plasmid, and MD145 (GII.4) strains into the Gateway® pDONR221 entry plasmid . N-terminal Renilla reniformis Luciferase (RL) and *S. aureus* protein A (PA) fusion protein plasmids were generated in pcDNA3-RL-GW and pTrex-Dest30-PA expression vectors respectively using the Gateway® Clonase® II enzyme recombination system (Invitrogen). The negative control plasmid consisted of a double protein A fusion protein (PA-PA). Validation of LUMIER assays was performed using positive control plasmids consisting of RL-c-Jun and PA-c-Fos fusion proteins.

Antibodies

Recombinant NS6 from GI.1, GII.4 and MNV was prepared in E. coli as described previously (46), combined, and used as antigen for preparation of rabbit polyclonal antisera. The resulting sera was affinity purified against MNV NS6. NS3, NS5 (VPg) and NS7 antibodies were prepared in our laboratory previously, and anti-NS5 was affinity purified against Cherry-tagged MNV NS5. Antisera to

GAPDH (Ambion), VDAC (Abcam), PABP (Cell Signaling), GFP (Abcam) were purchased from the indicated vendors.

Western blotting

Cells were lysed in RIPA buffer (50mM Tris pH8, 150mM NaCl, 1mM EDTA, 1% Triton X-100, 0.1% SDS) and protein concentrations determined by BCA assay (Pierce). Samples were then mixed with SDS sample loading buffer. We and others (Eoin Leen, personal communication) have observed that heating samples containing NS6, or some of the other NS6-containing precursors can cause these to precipitate in the sample buffer. As such blotting was performed by mixing the sample with SDS sample loading buffer and then immediately loading the sample onto the gel without heating. Samples were supplemented with RNase cocktail, and the use of lower sample concentrations (3-5µg/well) also helped prevent smearing. Samples were run on SDS-PAGE gels, transferred to nitrocellulose membranes, blocked and probed by standard protocols. Detection was accomplished using IR-dye 680 or 800-conjugated secondary antibodies followed by imaging on a Li-Cor Odyssey imager.

Confocal Microscopy

Cells were grown on glass coverslips, transfected, and infected as indicated above. At the relevant timepoint, the coverslips were washed with cold PBS, fixed in 4% paraformaldehyde in PBS for 10 min on ice, and permeabilized with PBS containing 0.2% Triton X-100 and 4% paraformaldehyde for an additional 10 min at room temperature. Aldehyde groups were quenched with 0.2 M glycine in PBS. Subsequent antibody incubations and washing steps followed

standard protocols and have been described previously (47). Alexa-fluor fluorescent secondary antibodies were obtained from Molecular Probes and used at the manufacturers recommended dilution. Coverslips were mounted on glass slides using Mowiol supplemented with DAPI. Imaging was performed on a Leica Sp5 confocal microscope using a 63x oil objective. Image analysis was performed in the Leica Lite software (Leica Microsystems).

In vitro translation reactions

In vitro translation assays were performed with 1ug template plasmid and the T7 coupled *in vitro* transcription-translation kit (Promega). Reactions were either performed with ^{35}S-methionine labeling, or unlabeled as indicated in the text. Half-size reactions (25µl) reactions were incubated at 30°C for 1h 30m. At the end of the incubation the reactions were mixed with an equal volume of Trans-stop buffer (10mM EDTA, 100ng/ml RNAse A) and incubated at room temperature for 30m.

For experiments assessing cleavage of ^{35}S-methionine labeled substrate by unlabeled protease/precursors, after addition of trans-stop, 5µl of labeled substrate was mixed with 15µl of unlabeled protease. This was then mixed with 4 volumes (80µl) of protease assay buffer (10mM HEPES pH7.6, 0.1% CHAPS, 10mM DTT and 30% glycerol (46)) and incubated at 37°C for 48 hours.

All samples were then combined with reducing SDS-PAGE loading buffer, resolved on a denaturing 17.5% SDS-PAGE gel, dried, and imaged using a Typhoon FLA 7000 phosphorimager.

644

645 LUMIER assay

646 All assays were performed in quadruplicate. 96 well plates containing 5 x 10^4
647 HEK-293T cells per well in 100µl of DMEM supplemented with 15% FBS were
648 seeded 12h prior transfection. Co-transfections were performed with 60ng of
649 combined bait and prey plasmids with 0.3µl lipofectamine 2000 (Invitrogen) in
650 30µl Opti-MEM I (Gibco) per well. After 24h incubation, cells were lysed for 10
651 min at 4°C with shaking using 30µl of ice-cold LUMIER lysis buffer (PBS pH 7.4
652 (Mg/Ca free), 1% Triton X100, 0.1% BSA, 1mM DTT) with 1% Halt EDTA-free
653 Protease/Phosphatase Inhibitor Cocktail (Pierce) and benzonase nuclease
654 (Novagen)) Each supernatant was transferred in a 96 well V-bottom plate, and
655 then centrifuged at 2000 x *g* for 15 min at 4°C. 20µl of each supernatant was
656 retained and transferred to a new white flat bottom plate.

657

658 Dynabeads M280 sheep anti-rabbit IgG-coated magnetic beads (Invitrogen) were
659 washed 3 times with the LUMIER washing buffer (PBS pH 7.4 (Mg/Ca free), 0.1%
660 BSA, 1mM DTT, 1mM ATP) then coupled overnight at 4°C with a polyclonal anti-
661 protein A rabbit antibody (Sigma-Aldrich). The beads were washed 4 times with
662 LUMIER washing buffer. 2µl of beads in 30µl of LUMIER washing buffer was
663 added to each well containing the lysate supernatents.

664

665 After 90 min of incubation on shaker at 4°C, 60µl of LUMIER washing buffer was
666 added to each plate and mixed. After transferring 10µl of supernatant per well to
667 new 96-well white plates plates to measure unbound activity, IP plates were
668 washed six times with LUMIER washing buffer. Renilla luciferase activity was

669 measured in both IP and unbound plates on a GloMax luminometer (Promega).
670 Data were normalised to background ratios and Robust Z-score (RZ) calculated
671 (48).
672

673 ## Acknowledgements

674 IG is supported by a Wellcome Trust Senior Fellowship (WT097997MA). This
675 work was also supported by the Cambridge NIHR BRC cell phenotyping hub, who
676 are thanked for their assistance with microscopy.
677
678

679 # References

680 1. Jones, M. K., Watanabe, M., Zhu, S., Graves, C. L., Keyes, L. R., Grau, K. R.,
681 Gonzalez-Hernandez, M. B., Iovine, N. M., Wobus, C. E., Vinje, J., Tibbetts, S.
682 A., Wallet, S. M., and Karst, S. M. (2014) Enteric bacteria promote human
683 and mouse norovirus infection of B cells. *Science.* **346**, 755–759
684 2. Ettayebi, K., Crawford, S. E., Murakami, K., Broughman, J. R., Karandikar, U.,
685 Tenge, V. R., Neill, F. H., Blutt, S. E., Zeng, X.-L., Qu, L., Kou, B., Opekun, A. R.,
686 Burrin, D., Graham, D. Y., Ramani, S., Atmar, R. L., and Estes, M. K. (2016)
687 Replication of human noroviruses in stem cell–derived human enteroids.
688 *Science.* **353**, 1387–1393
689 3. Karst, S. M., Wobus, C. E., Lay, M., Davidson, J., and Virgin, H. W. (2003)
690 STAT1-dependent innate immunity to a Norwalk-like virus. *Science*. **299**,
691 1575–8
692 4. Karst, S. M., and Wobus, C. E. (2015) Viruses in Rodent Colonies: Lessons
693 Learned from Murine Noroviruses. *Annu. Rev. Virol.* **2**, 525–548
694 5. Karst, S. M., and Tibbetts, S. A. (2016) Recent advances in understanding
695 norovirus pathogenesis. *J. Med. Virol.* **88**, 1837–1843
696 6. Sosnovtsev, S. V, Belliot, G., Chang, K.-O., Prikhodko, V. G., Thackray, L. B.,
697 Wobus, C. E., Karst, S. M., Virgin, H. W., and Green, K. Y. (2006) Cleavage
698 map and proteolytic processing of the murine norovirus nonstructural
699 polyprotein in infected cells. *J. Virol.* **80**, 7816–31
700 7. Emmott, E., Sweeney, T. R., and Goodfellow, I. (2015) A Cell-Based FRET
701 Sensor Reveals Inter- and Intragenogroup Variation in Norovirus Protease
702 Activity and Polyprotein Cleavage. *J. Biol. Chem.* **290**, jbc.M115.688234
703 8. Cameron, C. E., Oh, H. S., and Moustafa, I. M. (2010) Expanding knowledge

of P3 proteins in the poliovirus lifecycle. *Future Microbiol.* **5**, 867–81

9. Scheffler, U., Rudolph, W., Gebhardt, J., and Rohayem, J. (2007) Differential cleavage of the norovirus polyprotein precursor by two active forms of the viral protease. *J. Gen. Virol.* **88**, 2013–8

10. Belliot, G., Sosnovtsev, S. V, Chang, K.-O., Babu, V., Uche, U., Arnold, J. J., Cameron, C. E., and Green, K. Y. (2005) Norovirus proteinase-polymerase and polymerase are both active forms of RNA-dependent RNA polymerase. *J. Virol.* **79**, 2393–403

11. Wei, L., Huhn, J. S., Mory, A., Pathak, H. B., Sosnovtsev, S. V, Green, K. Y., and Cameron, C. E. (2001) Proteinase-polymerase precursor as the active form of feline calicivirus RNA-dependent RNA polymerase. *J. Virol.* **75**, 1211–9

12. Pathak, H. B., Oh, H. S., Goodfellow, I. G., Arnold, J. J., and Cameron, C. E. (2008) Picornavirus genome replication: roles of precursor proteins and rate-limiting steps in oriI-dependent VPg uridylylation. *J. Biol. Chem.* **283**, 30677–88

13. Shirako, Y., and Strauss, J. H. (1994) Regulation of Sindbis virus RNA replication: uncleaved P123 and nsP4 function in minus-strand RNA synthesis, whereas cleaved products from P123 are required for efficient plus-strand RNA synthesis. *J. Virol.* **68**, 1874–85

14. Emmott, E., Sorgeloos, F., Caddy, S. L., Vashist, S., Sosnovtsev, S., Lloyd, R., Heesom, K., Locker, N., and Goodfellow, I. (2017) Norovirus-Mediated Modification of the Translational Landscape via Virus and Host-Induced Cleavage of Translation Initiation Factors. *Mol. Cell. proteomics*. **16**, S215–S229

15. Thorne, L. G., and Goodfellow, I. G. (2014) Norovirus gene expression and

729 replication. *J. Gen. Virol.* **95**, 278–91

730 16. Chung, L., Bailey, D., Leen, E. N., Emmott, E. P., Chaudhry, Y., Roberts, L. O.,
731 Curry, S., Locker, N., and Goodfellow, I. G. (2014) Norovirus translation
732 requires an interaction between the C Terminus of the genome-linked viral
733 protein VPg and eukaryotic translation initiation factor 4G. *J. Biol. Chem.*
734 **289**, 21738–50

735 17. Olspert, A., Hosmillo, M., Chaudhry, Y., Peil, L., Truve, E., and Goodfellow, I.
736 (2016) Protein-RNA linkage and posttranslational modifications of feline
737 calicivirus and murine norovirus VPg proteins. *PeerJ*. **4**, e2134

738 18. Hyde, J. L., and Mackenzie, J. M. (2010) Subcellular localization of the MNV-
739 1 ORF1 proteins and their potential roles in the formation of the MNV-1
740 replication complex. *Virology*. **406**, 138–148

741 19. Nice, T. J., Strong, D. W., McCune, B. T., Pohl, C. S., and Virgin, H. W. (2013) A
742 Single-Amino-Acid Change in Murine Norovirus NS1/2 Is Sufficient for
743 Colonic Tropism and Persistence. *J. Virol.* **87**, 327–334

744 20. Pfister, T., and Wimmer, E. (2001) Polypeptide p41 of a Norwalk-Like
745 Virus Is a Nucleic Acid-Independent Nucleoside Triphosphatase. *J. Virol.*
746 **75**, 1611–1619

747 21. Cotton, B. T., Hyde, J. L., Sarvestani, S. T., Sosnovtsev, S. V, Green, K. Y.,
748 White, P. A., and Mackenzie, J. M. (2017) The Norovirus NS3 Protein Is a
749 Dynamic Lipid- and Microtubule-Associated Protein Involved in Viral RNA
750 Replication. *J. Virol.* **91**, e02138–16

751 22. Rocha-Pereira, J., Van Dycke, J., and Neyts, J. (2016) Norovirus genetic
752 diversity and evolution: implications for antiviral therapy. *Curr. Opin. Virol.*
753 **20**, 92–98

754 23. Arias, A., Emmott, E., Vashist, S., and Goodfellow, I. (2013) Progress
755 towards the prevention and treatment of norovirus infections. *Future*
756 *Microbiol.* **8**, 1475–1487
757 24. Haga, K., Fujimoto, A., Takai-Todaka, R., Miki, M., Doan, Y. H., Murakami, K.,
758 Yokoyama, M., Murata, K., Nakanishi, A., and Katayama, K. (2016)
759 Functional receptor molecules CD300lf and CD300ld within the CD300
760 family enable murine noroviruses to infect cells. *Proc. Natl. Acad. Sci. U. S.*
761 *A.* **113**, E6248–E6255
762 25. Orchard, R. C., Wilen, C. B., Doench, J. G., Baldridge, M. T., McCune, B. T., Lee,
763 Y.-C. J., Lee, S., Pruett-Miller, S. M., Nelson, C. A., Fremont, D. H., and Virgin,
764 H. W. (2016) Discovery of a proteinaceous cellular receptor for a
765 norovirus. *Science*. **353**, 933–6
766 26. Hyde, J. L., Sosnovtsev, S. V., Green, K. Y., Wobus, C., Virgin, H. W., and
767 Mackenzie, J. M. (2009) Mouse Norovirus Replication Is Associated with
768 Virus-Induced Vesicle Clusters Originating from Membranes Derived from
769 the Secretory Pathway. *J. Virol.* **83**, 9709–9719
770 27. Holden, P., and Horton, W. A. (2009) Crude subcellular fractionation of
771 cultured mammalian cell lines. *BMC Res. Notes*. **2**, 243
772 28. Schechter, I., and Berger, A. (1967) On the size of the active site in
773 proteases. I. Papain. *Biochem. Biophys. Res. Commun.* **27**, 157–62
774 29. Barrios-Rodiles, M., Brown, K. R., Ozdamar, B., Bose, R., Liu, Z., Donovan, R.
775 S., Shinjo, F., Liu, Y., Dembowy, J., Taylor, I. W., Luga, V., Przulj, N., Robinson,
776 M., Suzuki, H., Hayashizaki, Y., Jurisica, I., and Wrana, J. L. (2005) High-
777 Throughput Mapping of a Dynamic Signaling Network in Mammalian Cells.
778 *Science.* **307**, 1621–1625

30. Barrios-Rodiles, M., Ellis, J. D., Blencowe, B. J., and Wrana, J. L. (2017) LUMIER: A Discovery Tool for Mammalian Protein Interaction Networks. in *Methods in molecular biology (Clifton, N.J.)*, pp. 137–148, **1550**, 137–148

31. Bailey, D., Kaiser, W. J., Hollinshead, M., Moffat, K., Chaudhry, Y., Wileman, T., Sosnovtsev, S. V., and Goodfellow, I. G. (2010) Feline calicivirus p32, p39 and p30 proteins localize to the endoplasmic reticulum to initiate replication complex formation. *J. Gen. Virol.* **91**, 739–749

32. Subba-Reddy, C. V., Goodfellow, I., and Kao, C. C. (2011) VPg-Primed RNA Synthesis of Norovirus RNA-Dependent RNA Polymerases by Using a Novel Cell-Based Assay. *J. Virol.* **85**, 13027–13037

33. May, J., Korba, B., Medvedev, A., and Viswanathan, P. (2013) Enzyme kinetics of the human norovirus protease control virus polyprotein processing order. *Virology*. **444**, 218–24

34. Medvedev, A., Viswanathan, P., May, J., and Korba, B. (2017) Regulation of human norovirus VPg nucleotidylylation by ProPol and nucleoside triphosphate binding by its amino terminal sequence in vitro. *Virology*. **503**, 37–45

35. Reid, C., Airo, A., and Hobman, T. (2015) The Virus-Host Interplay: Biogenesis of +RNA Replication Complexes. *Viruses*. **7**, 4385–4413

36. den Boon, J. A., Diaz, A., Ahlquist, P., Nibert, M. L., Baker, T. S., Walther, P., Fuller, S. D., Antony, C., Krijnse-Locker, J., Bartenschlager, R., and al., et (2010) Cytoplasmic viral replication complexes. *Cell Host Microbe*. **8**, 77–85

37. Kaiser, W. J., Chaudhry, Y., Sosnovtsev, S. V, and Goodfellow, I. G. (2006) Analysis of protein-protein interactions in the feline calicivirus replication

complex. *J. Gen. Virol.* **87**, 363–368

38. Vashist, S., Urena, L., and Goodfellow, I. (2012) Development of a strand specific real-time RT-qPCR assay for the detection and quantitation of murine norovirus RNA. *J. Virol. Methods*. **184**, 69–76

39. Rohayem, J., Robel, I., Jager, K., Scheffler, U., and Rudolph, W. (2006) Protein-Primed and De Novo Initiation of RNA Synthesis by Norovirus 3Dpol. *J. Virol.* **80**, 7060–7069

40. Subba-Reddy, C. V, Yunus, M. A., Goodfellow, I. G., and Kao, C. C. (2012) Norovirus RNA synthesis is modulated by an interaction between the viral RNA-dependent RNA polymerase and the major capsid protein, VP1. *J. Virol.* **86**, 10138–49

41. Oh, H. S., Pathak, H. B., Goodfellow, I. G., Arnold, J. J., and Cameron, C. E. (2009) Insight into Poliovirus Genome Replication and Encapsidation Obtained from Studies of 3B-3C Cleavage Site Mutants. *J. Virol.* **83**, 9370–9387

42. Leen, E. N., Sorgeloos, F., Correia, S., Chaudhry, Y., Cannac, F., Pastore, C., Xu, Y., Graham, S. C., Matthews, S. J., Goodfellow, I. G., and Curry, S. (2016) A Conserved Interaction between a C-Terminal Motif in Norovirus VPg and the HEAT-1 Domain of eIF4G Is Essential for Translation Initiation. *PLoS Pathog.* **12**, e1005379

43. Chaudhry, Y., Skinner, M. A., and Goodfellow, I. G. (2007) Recovery of genetically defined murine norovirus in tissue culture by using a fowlpox virus expressing T7 RNA polymerase. *J. Gen. Virol.* **88**, 2091–100

44. Hwang, S., Alhatlani, B., Arias, A., Caddy, S. L., Christodoulou, C., Cunha, J. B., Emmott, E., Gonzalez-Hernandez, M., Kolawole, A., Lu, J., Rippinger, C.,

Sorgeloos, F., Thorne, L., Vashist, S., Goodfellow, I., and Wobus, C. E. (2014) Murine norovirus: propagation, quantification, and genetic manipulation. *Curr. Protoc. Microbiol.* **33**, 15K.2.1–15K.2.61

45. Arias, A., Ureña, L., Thorne, L., Yunus, M. A., and Goodfellow, I. (2012) Reverse genetics mediated recovery of infectious murine norovirus. *J. Vis. Exp.* 10.3791/4145

46. Viswanathan, P., May, J., Uhm, S., Yon, C., and Korba, B. (2013) RNA binding by human Norovirus 3C-like proteases inhibits protease activity. *Virology*. **438**, 20–7

47. Vashist, S., Urena, L., Chaudhry, Y., and Goodfellow, I. (2012) Identification of RNA-protein interaction networks involved in the norovirus life cycle. *J. Virol.* **86**, 11977–90

48. Malo, N., Hanley, J. A., Cerquozzi, S., Pelletier, J., and Nadon, R. (2006) Statistical practice in high-throughput screening data analysis. *Nat. Biotechnol.* **24**, 167–175

847 **Figure legends:**

848 **Figure 1. Norovirus protease produced during authentic viral replication**
849 **inefficiently cleaves a cytoplasmic-localized protease substrate.** A) Genome
850 schematic of the murine norovirus genome highlighting the major open reading
851 frames and the components of the polyprotein. B) Schematic of the CFP-YFP
852 FRET sensor highlighting the NS1/2-NS3 boundary cleavage site. C) Western blot
853 analysis of HEK-293T cells co-transfected with the FRET sensor and either wild-
854 type or catalytically inactive protease (WT and H30A respectively), or BV-2 cells
855 electroporated with *in vitro* transcribed RNA encoding the FRET sensor and
856 subsequently infected at MOI 10 $TCID_{50}$/cell with MNV for 9h. Higher molecular
857 weight NS6 containing isoforms produced during viral infection are indicated
858 with asterisks. Note that the left and right-hand regions of the NS6 western blot
859 were imaged at different intensities to compensate for the lower NS6 signal
860 intensity in infected cells. D) Confocal microscopy of HeLa-CD300lf cells
861 transfected with the FRET sensor and either co-transfected with an NS6
862 expression construct (NS6) and harvested at 18h post-transfection, or infected
863 with MNV (+MNV) at a MOI of 10 $TCID_{50}$/cell at 6h post-transfection, and
864 harvested at 12h post-infection. The FRET sensor was visualized in the CFP and
865 YFP channels, the protease with antisera against NS6, and nuclei stained with
866 DAPI.

867

868 **Figure 2. Targeting protease substrates to the norovirus replication**
869 **complex enhances cleavage by NS6.** A) Western blotting of cells BSR-T7 cells
870 transfected with either proteolytically active (MNV-FLC) or inactive (MNV-
871 H30A) full-length infectious MNV clone, or polyprotein fused to the FRET sensor

(ORF1-FRET-WT, ORF1-FRET-H30A). Samples were lysed at 18h post-transfection. B) Confocal microscopy of BSR-T7 cells fixed at 18h post-transfection with ORF1-FRET-WT or ORF1-FRET-H30A constructs. The FRET substrate was visualized in the CFP and YFP channels, and nuclei stained with DAPI.

Figure 3. Accumulation of polyprotein precursors during MNV infection. BV-2 cells were infected at a MOI of 10 $TCID_{50}$/cell, and harvested at the indicated times post-infection. Western blot analysis with antisera against A) NS6 or B) NS5/VPg revealed the high levels of precursor proteins present at early stages of infection. To ensure efficient transfer and resolution of the various precursors, samples were separated on both 7.5% (upper) and 17.5% (lower) SDS-PAGE gels prior to transfer and western blot. C) Infectious virus produced across the timecourse was determined by $TCID_{50}$ following freeze-thaw to release intracellular virus. D) To investigate precursor localization, BV-2 cells were infected at MOI 10 and harvested at 9h post-infection where they were subject to fractionation into soluble cytoplasmic, and cytoplasmic membrane-associated fractions. Lysates were blotted for viral and cellular markers as indicated.

Figure 4. Activity of NS6-containing stable precursors. FLAG-tagged forms of the various protease-containing precursors were generated by mutagenesis of the P1 residue at each cleavage site to an alanine. A H30A mutation within the protease abolished proteolytic activity. A) A schematic illustrating the 10 possible NS6-containing precursors generated by NS6 cleavage of the

polyprotein. Protease-containing precursors may all be observed following B) *in vitro* translation of the precursors incorporating ^{35}S Met labeling followed by phosphorimaging, or C) Expression in BSR-T7 cells visualized by western blotting. Incubation of unlabeled *in vitro* translated precursors with ^{35}S Methionine-labeled substrate demonstrates cleavage of the D) cellular substrate PABP. E) Western blotting of BSR-T7 cells harvested at 18h post-transfection with the precursors and FLAG-PABP reveals only a subset of precursors cleave PABP in cells. FLAG-tagged precursors are also visible on this image and are indicated with an asterisk (*). F) Western blotting of BSR-T7 cells co-expressing ORF1-FRET-H30A as substrate for trans-cleavage by co-expressed protease precursors shows cleavage of this substrate by all precursors at 18h post-transfection.

Figure 5. Confocal microscopy of protease precursors in mock or MNV-infected cells. HeLa-CD300lf cells were transfected with the various protease precursor constructs and at 6h post-transfection, mock- or infected with MNV at MOI 10. The cells were fixed and processed for microscopy at 12h post-infection. Nuclei were visualized with DAPI, the precursors with anti-FLAG antisera, and infected cells with anti-dsRNA antisera.

Figure 6. Components of the norovirus replication complex exhibit homo- and heteromeric interactions. HEK-293T cells expressing Protein-A and Renilla luciferase fusions of the various MNV proteins were used for LUMIER analysis to identify protein:protein interactions. The numbers are robust z-scores. Positive protein:protein interactions are coloured by the strength of

interaction with weak interactions showing in pale yellow, with the strongest interactions in purple. Protein expression was confirmed by western blotting (Figure S4).

Figure 7. Mutagenesis of polyprotein-FRET fusions reveals the importance of individual polyprotein components for replication complex targeting and substrate cleavage. A) Schematic illustrating the various N-, C- and internal deletion mutants generated from ORF1-FRET-H30A. These mutants were transfected into BSR-T7 cells to function as trans-cleavage substrates. WT or proteolytically-inactive full length clone (MNV-FLC, MNV-H30A) was provided *in trans* to determine cleavage efficiency. Samples were harvested at 18h post-transfection. B) N-terminal, C) C-terminal and D) Internal deletions are shown. Substrate cleavage was assessed using anti-GFP antisera. ORF1-FRET-WT was used as a positive control (+). For clarity the position of either the full length (Mock cells) or fully-processed cleavage product (MNV infected cells) is highlighted with a red asterisk (*).

Figure 8. Substrate targeting to the replication complex permits NS6 cleavage in infection. *In vitro* transcribed RNA encoding select truncation mutants of ORF1-FRET-H30A was electroporated into BV-2 cells. At 6h post-electroporation these cells were infected at MOI 10 and lysates prepared at A) 9h or B) 12h post-infection. Trans-cleavage of the substrate was determined by anti-GFP staining, and the presence of active protease provided *in trans* by anti-NS7 staining. For clarity the position of either the full length (Mock cells) or fully-

946 processed cleavage product (MNV infected cells) is highlighted with a red
947 asterisk (*).
948
949 **Figure S1. Confirmation of precursor identity in MNV-infected cell lysates.**
950 Lysates from BV-2 cells mock- or infected with MNV at MOI 10 and harvested at
951 9h post-infection, were compared to HEK-293T cell lysates mock- or transfected
952 with plasmids expressing stable forms of the various precursors. Precursors
953 were visualized by anti-NS6 and anti-NS5 antisera to assess co-migration. Note
954 that the addition of a FLAG-tag on the precursors adds at additional 1.14kDa
955 which results in some discrepancy in the migration of the smaller precursors.
956
957 **Figure S2. Confocal microscopy of N-terminal norovirus protease**
958 **precursors.** HeLa-CD300lf cells were transfected with plasmids expressing NS3-
959 6, NS3-7, NS1/2-6 and NS1/2-7. At 18h post-transfection the cells were
960 harvested and precursors visualized by anti-NS6 staining. Nuclei were visualized
961 with DAPI.
962
963 **Figure S3. Western blotting of MNV LUMIER assay reagents confirms**
964 **expression.** Western blotting of lysates prepared from HEK-293T cells
965 transfected with A) Renilla-luciferase or B) Protein-A fusions of the various MNV
966 proteins confirms their expression and migration at the expected size. Samples
967 were harvested at 24h post-transfection.
968
969 **Figure S4. LUMIER assay reveals GI.1 replication complex interactions are**
970 **conserved between GI.1 and MNV.** A) HEK-293T cells expressing Protein-A and

971 Renilla luciferase fusions of the various GI.1 human norovirus proteins were
972 used for LUMIER analysis to identify protein:protein interactions. The numbers
973 are robust z-scores. Positive protein:protein interactions are coloured by the
974 strength of interaction with weak interactions showing in pale yellow, with the
975 strongest interactions in purple. Western blotting of lysates prepared from HEK-
976 293T cells transfected with B) Renilla-luciferase or C) Protein-A fusions of the
977 various GI.1 norovirus proteins confirms their expression and migration at the
978 expected size. Samples were harvested at 24h post-transfection.
979
980 **Figure S5. LUMIER assay reveals GII.4 replication complex interactions are**
981 **conserved between GII.4 and MNV.** A) HEK-293T cells expressing Protein-A
982 and Renilla luciferase fusions of the various GII.4 human norovirus proteins were
983 used for LUMIER analysis to identify protein:protein interactions. The numbers
984 are robust z-scores. Positive protein:protein interactions are coloured by the
985 strength of interaction with weak interactions showing in pale yellow, with the
986 strongest interactions in purple. Western blotting of lysates prepared from HEK-
987 293T cells transfected with B) Renilla-luciferase or C) Protein-A fusions of the
988 various GII.4 norovirus proteins confirms their expression and migration at the
989 expected size. Samples were harvested at 24h post-transfection.
990
991 **Table S1. Predicted molecular weights of norovirus proteins and precursor**
992 **forms.** The first tab lists all the potential norovirus proteins and precursors that
993 can be derived from the polyprotein. The second and third tabs list all the NS5-
994 or NS6-containing precursors ranked by molecular weight from largest to

995 smallest. Predicted molecular weight was calculated using the ExPASy server
996 ProtParam tool.
997
998 **Supplemental Information:**
999 This manuscript has five supplementary figures and one supplementary table.
1000

Fig 1.

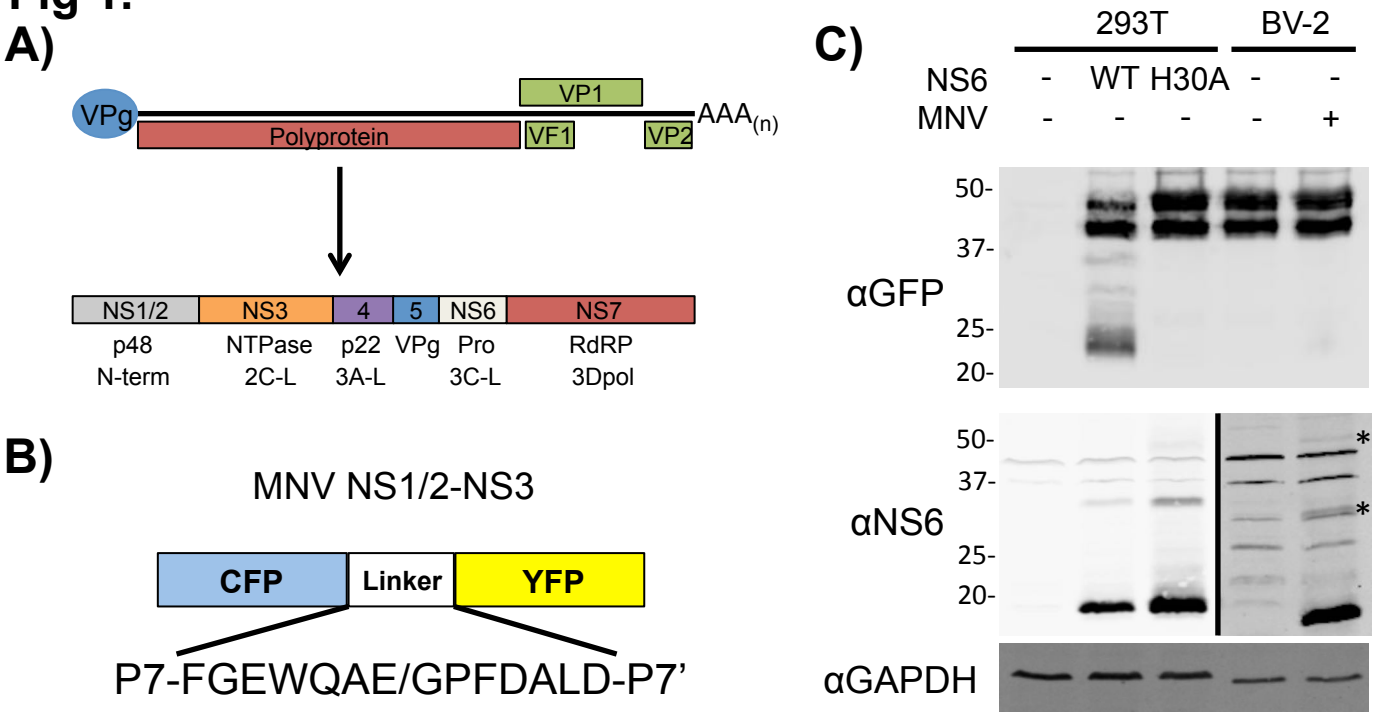

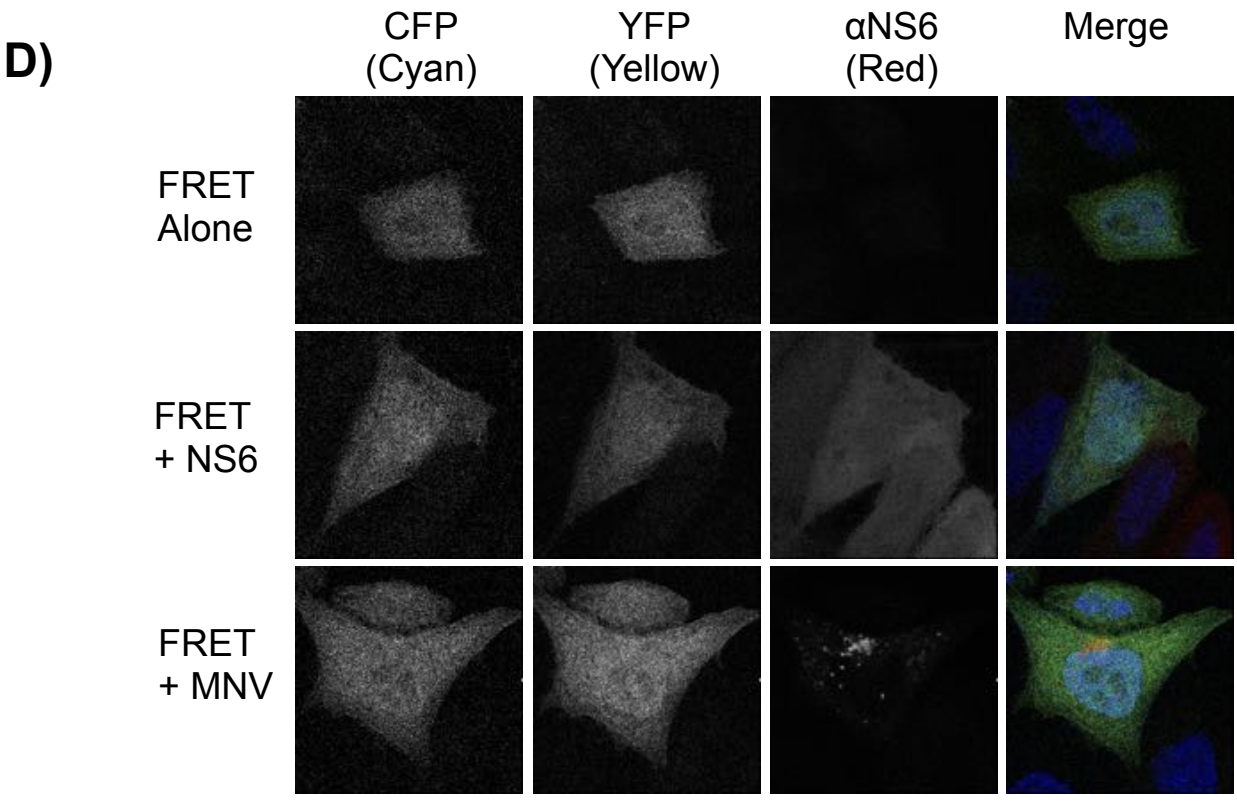

Fig 2.

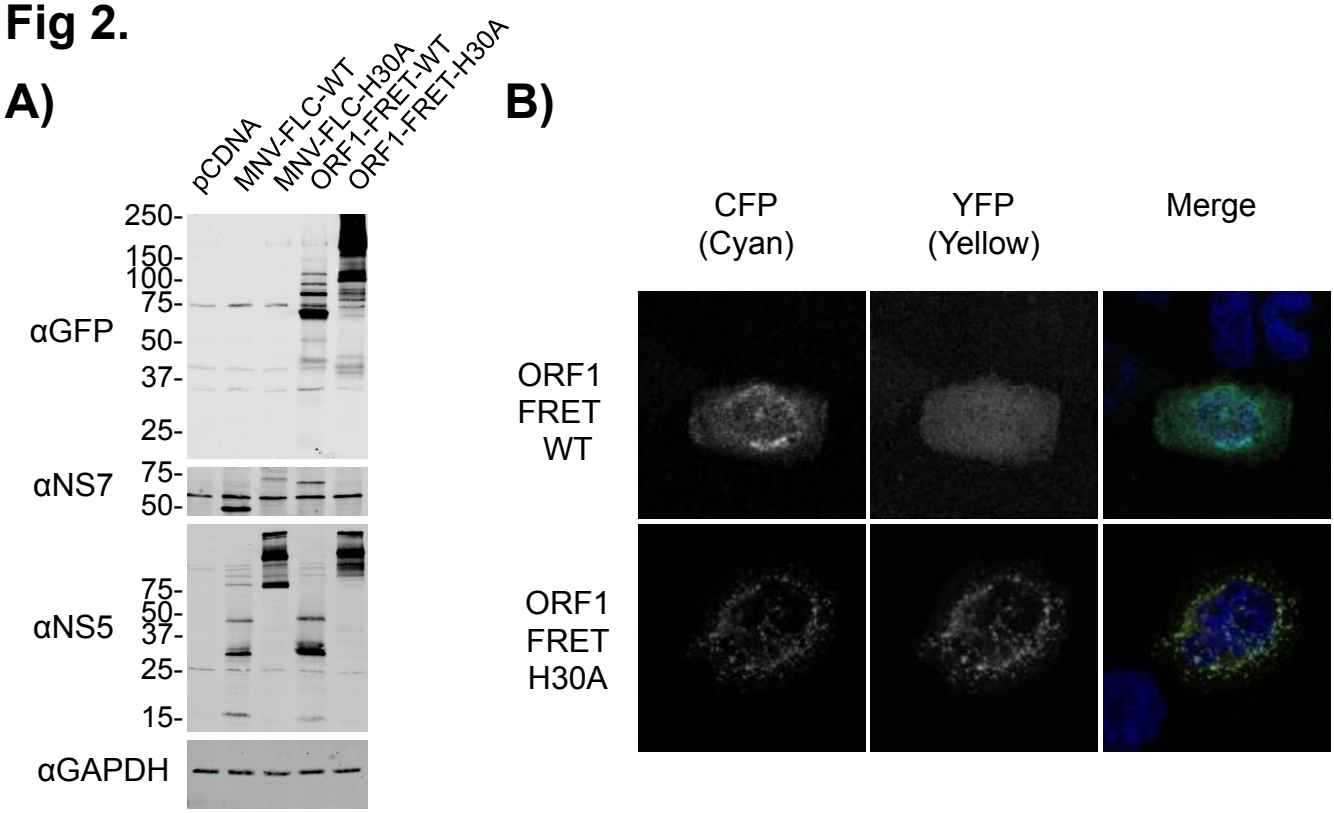

Fig 3.

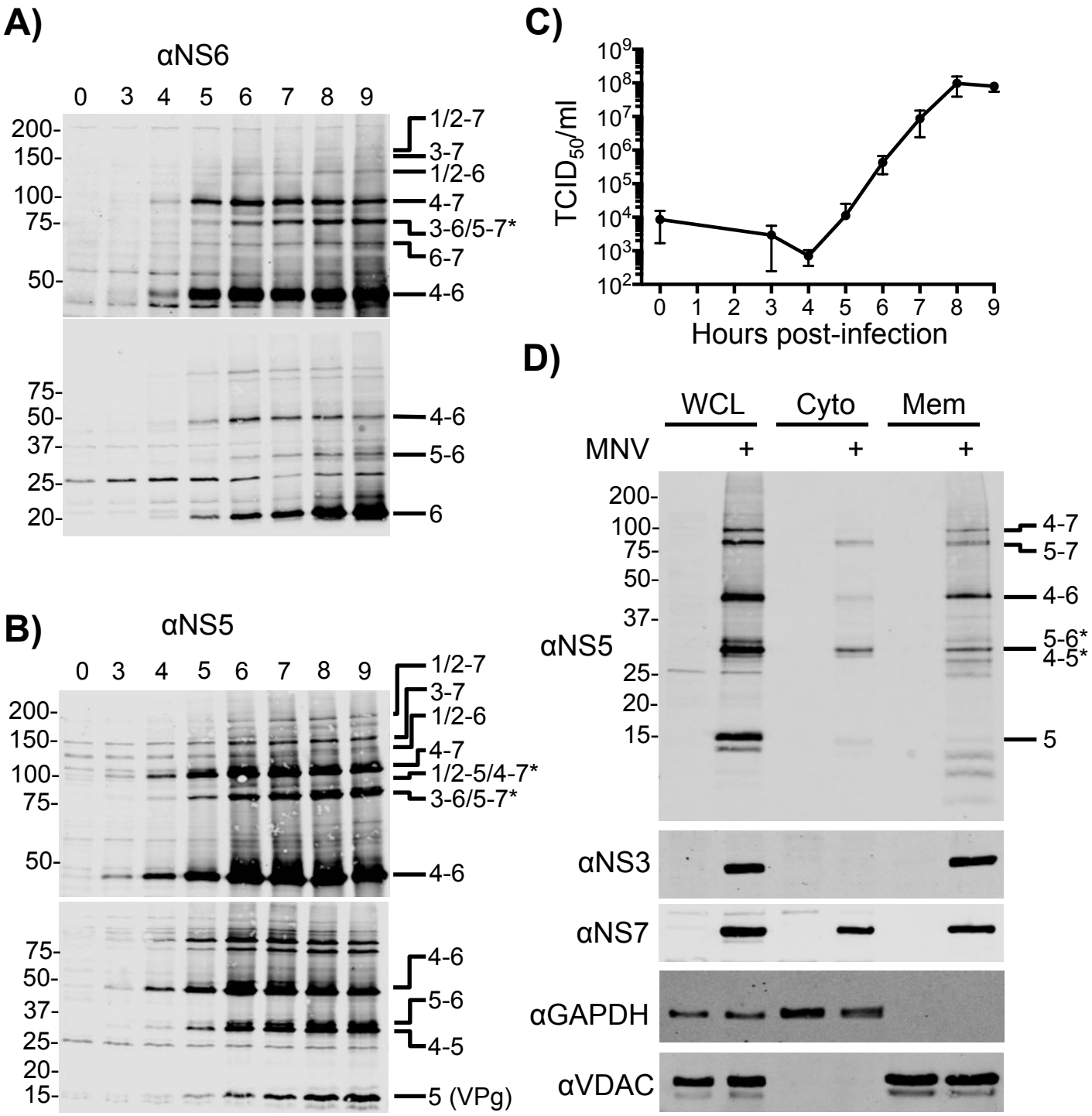

Fig 4.

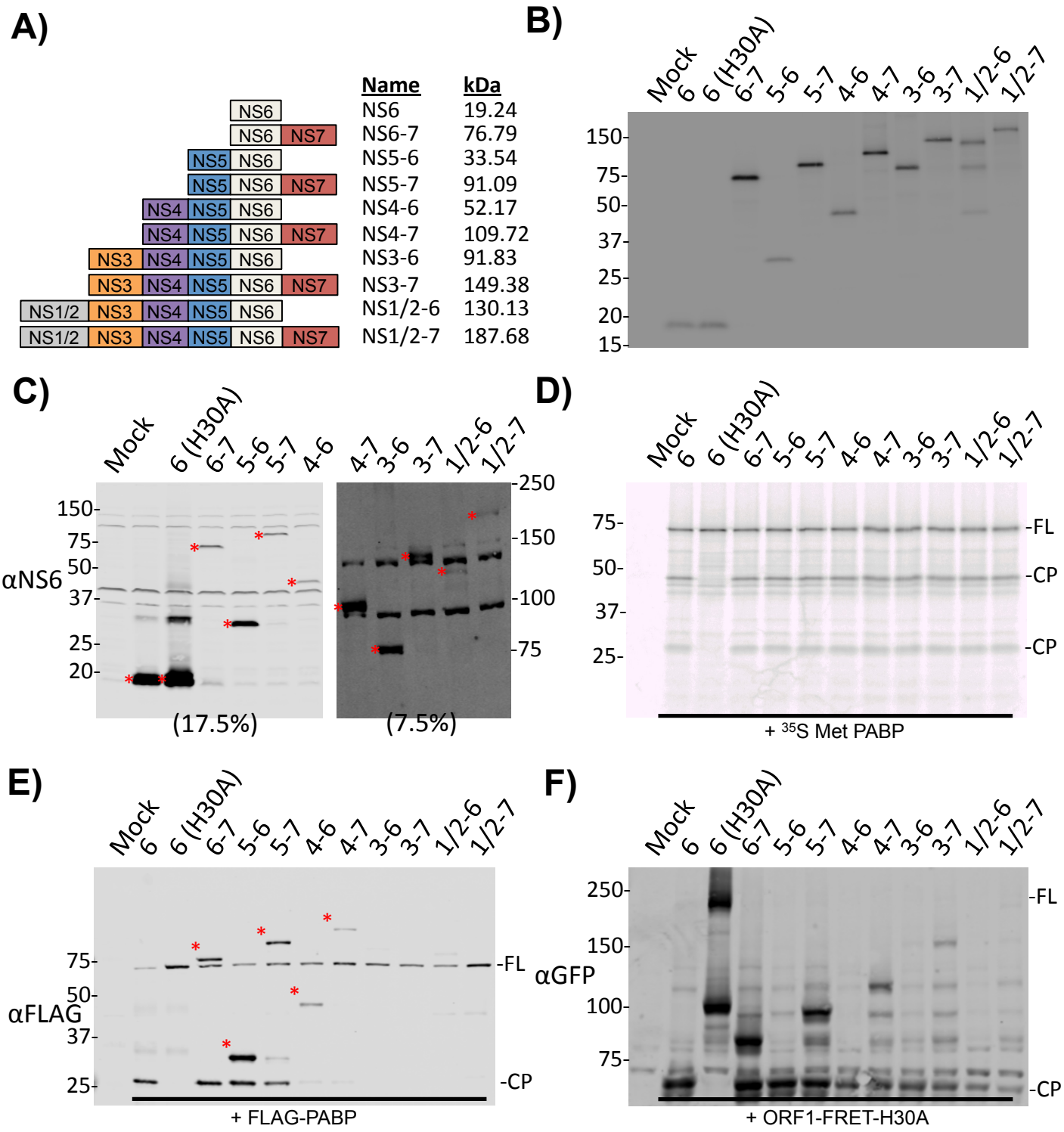

Fig 5.

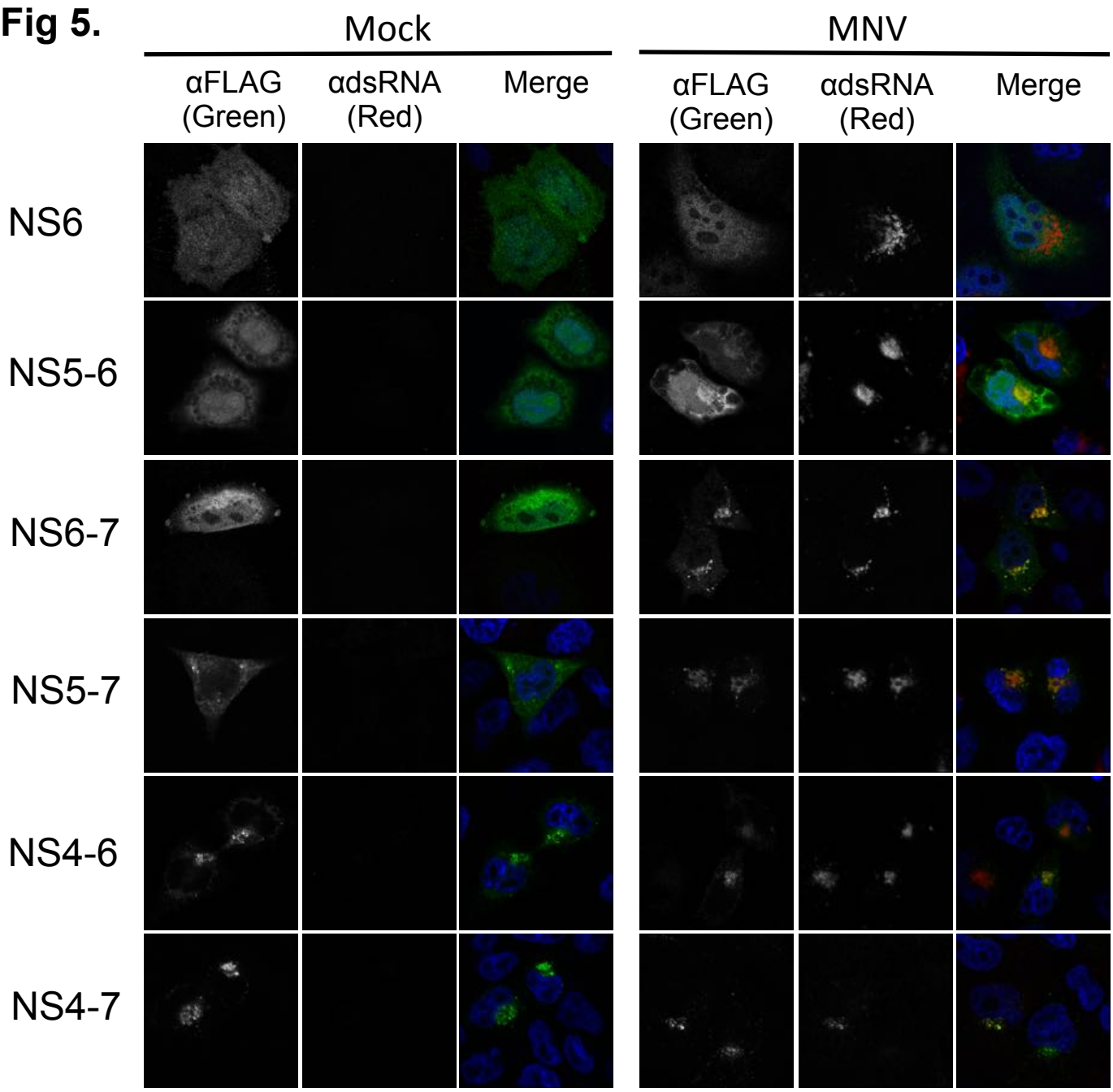

Fig 6.

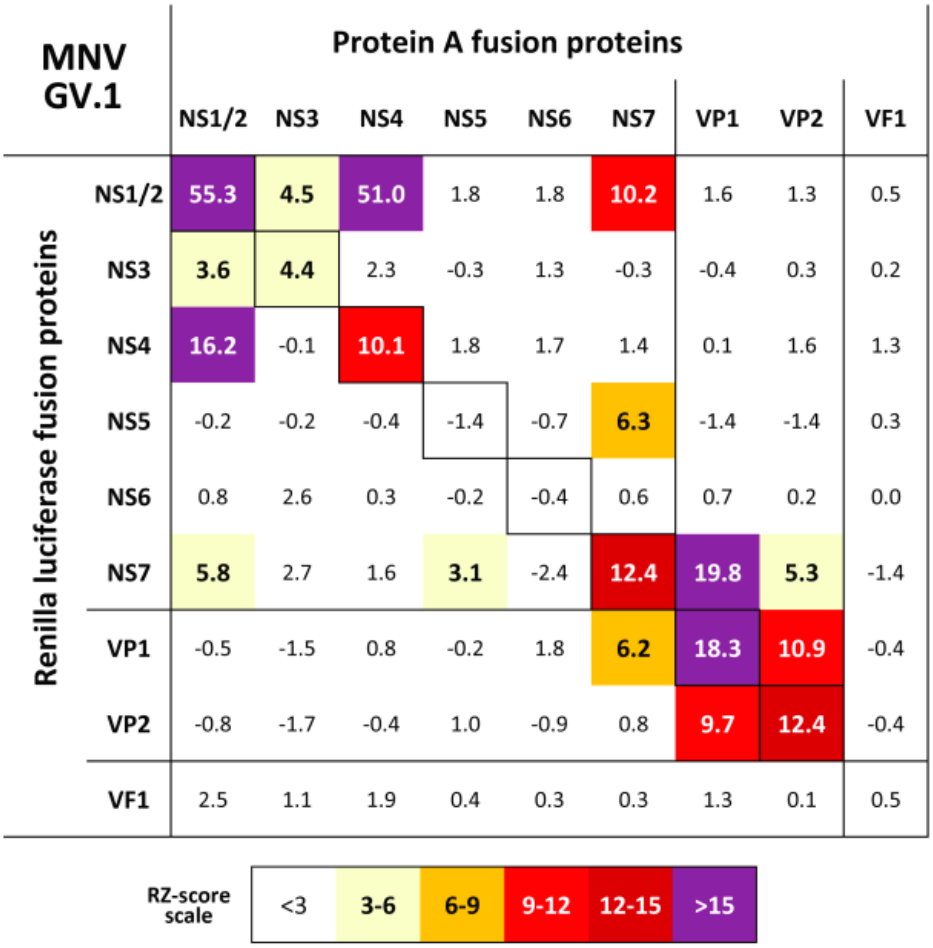

Fig 7.

A)

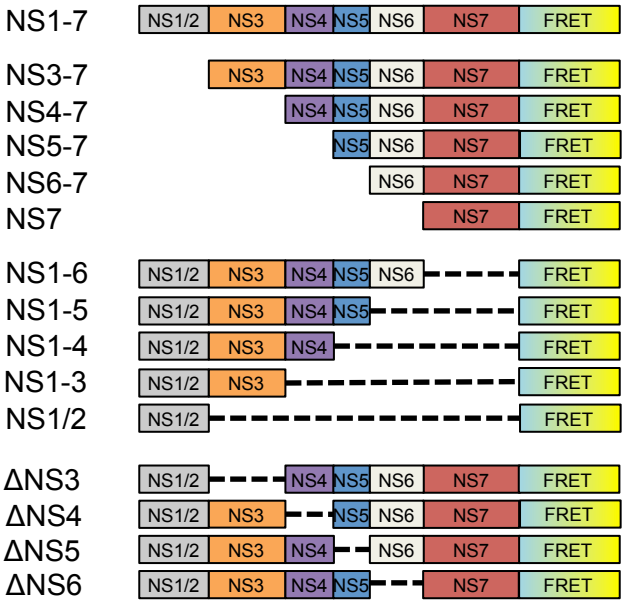
NS1-7
NS1/2 NS3 NS4 NS5 NS6 NS7 FRET
NS3-7
NS3 NS4 NS5 NS6 NS7 FRET
NS4-7
NS4 NS5 NS6 NS7 FRET
NS5-7
NS5 NS6 NS7 FRET
NS6-7
NS6 NS7 FRET
NS7
NS7 FRET
NS1-6
NS1/2 NS3 NS4 NS5 NS6 FRET
NS1-5
NS1/2 NS3 NS4 NS5 FRET
NS1-4
NS1/2 NS3 NS4 FRET
NS1-3
NS1/2 NS3 FRET
NS1/2
NS1/2 FRET
ΔNS3
NS1/2 NS4 NS5 NS6 NS7 FRET
ΔNS4
NS1/2 NS3 NS5 NS6 NS7 FRET
ΔNS5
NS1/2 NS3 NS4 NS6 NS7 FRET
ΔNS6
NS1/2 NS3 NS4 NS5 NS7 FRET

B)

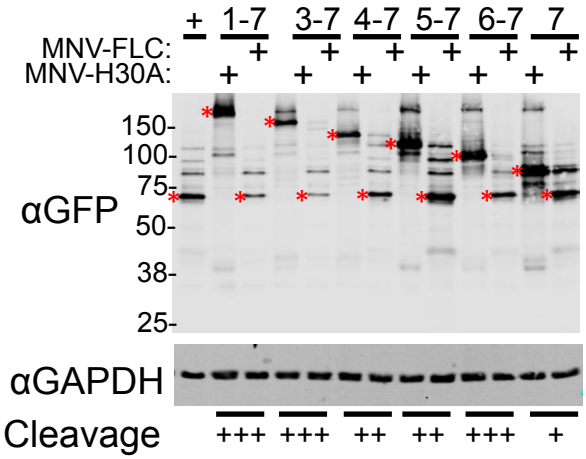
+ 1-7 3-7 4-7 5-7 6-7 7
MNV-FLC: + + + + + + +
MNV-H30A: + + + + + + +
150-
100-
75-
50-
38-
25-
αGFP
αGAPDH
Cleavage
+++ +++ ++ ++ +++ +

C)

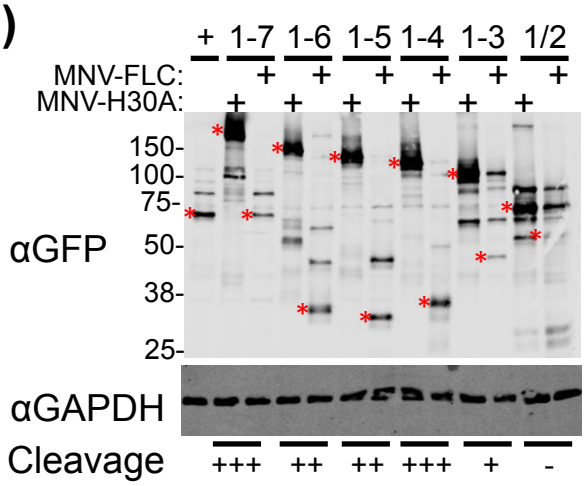
+ 1-7 1-6 1-5 1-4 1-3 1/2
MNV-FLC: + + + + + + +
MNV-H30A: + + + + + + +
150-
100-
75-
50-
38-
25-
αGFP
αGAPDH
Cleavage
+++ ++ ++ +++ + -

D)

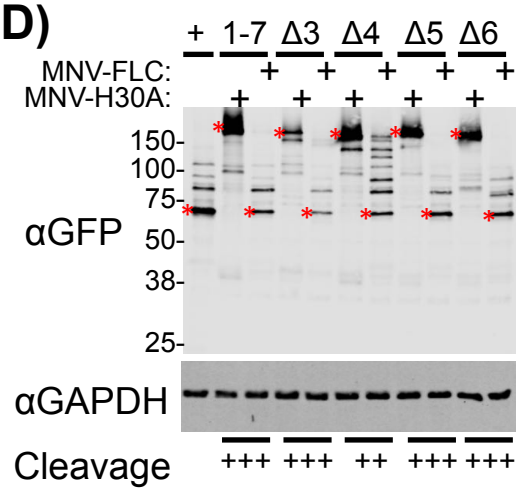
+ 1-7 Δ3 Δ4 Δ5 Δ6
MNV-FLC: + + + + + +
MNV-H30A: + + + + + +
150-
100-
75-
50-
38-
25-
αGFP
αGAPDH
Cleavage
+++ +++ ++ +++ +++

Fig 8.

A)

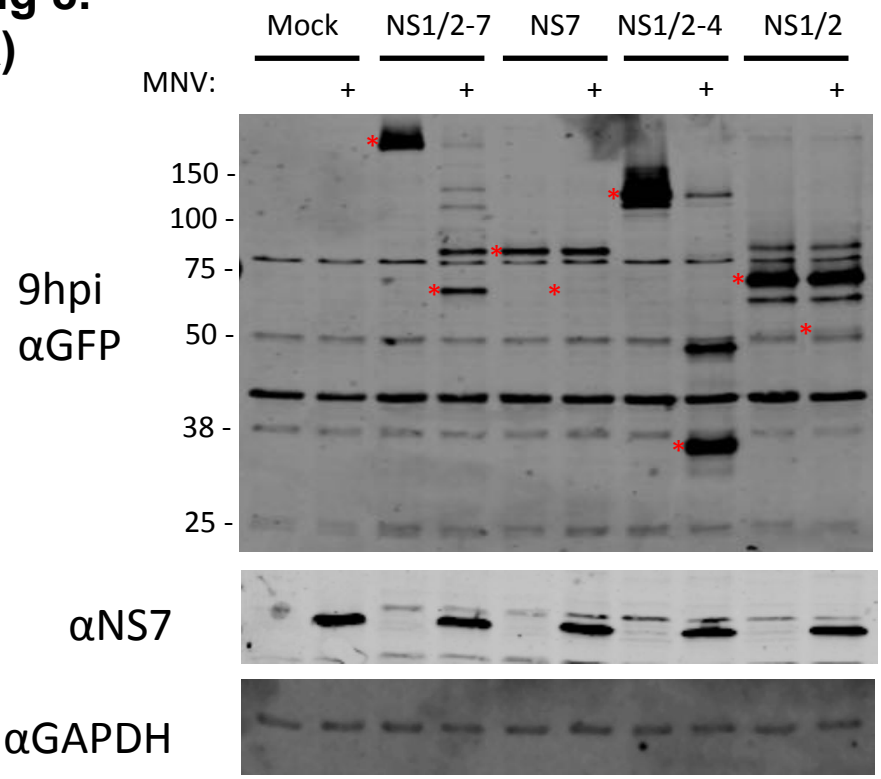
Mock
NS1/2-7
NS7
NS1/2-4
NS1/2
MNV:
+
+
+
+
+
150 -
100 -
75 -
50 -
38 -
25 -
9hpi
αGFP
αNS7
αGAPDH

B)

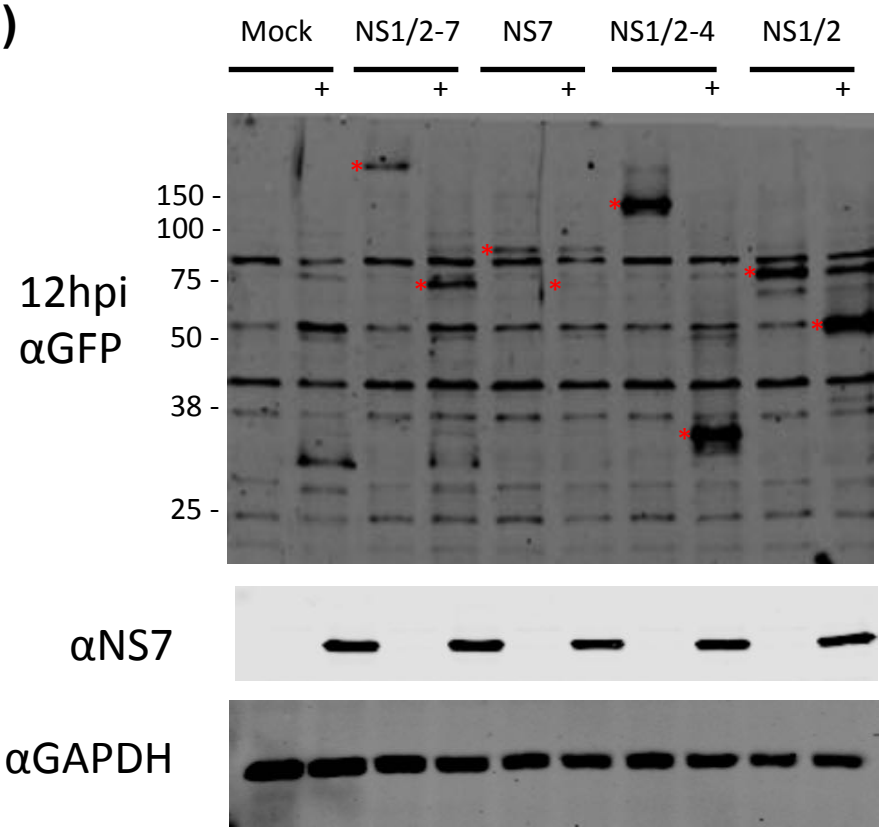
Mock
NS1/2-7
NS7
NS1/2-4
NS1/2
+
+
+
+
+
150 -
100 -
75 -
50 -
38 -
25 -
12hpi
αGFP
αNS7
αGAPDH

Fig S1.

A) NS6

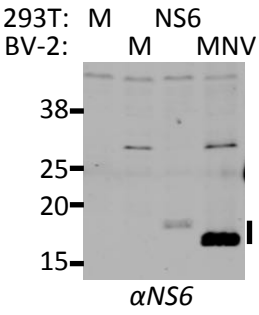

B) H30A

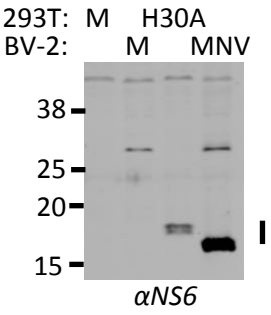

C) NS6-7

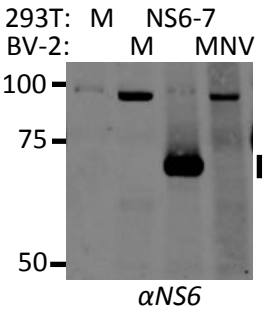

D) NS5-6

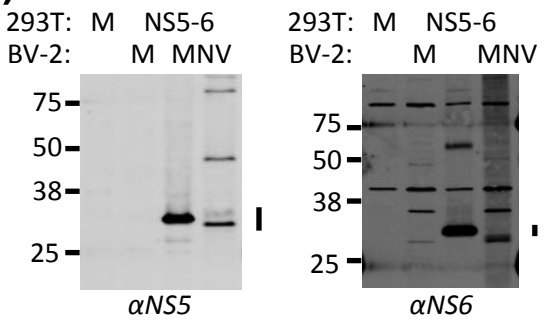

E) NS5-7

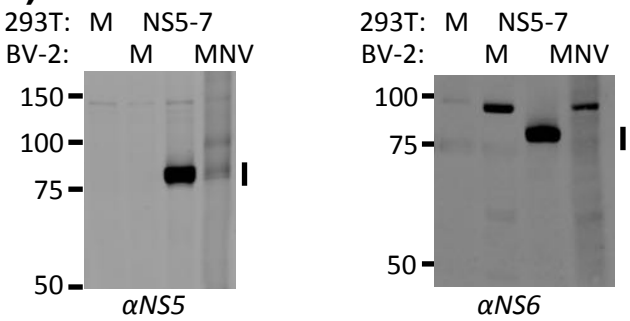

F) NS4-6

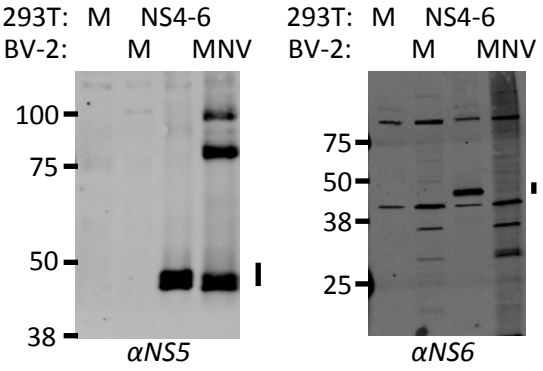

G) NS4-7

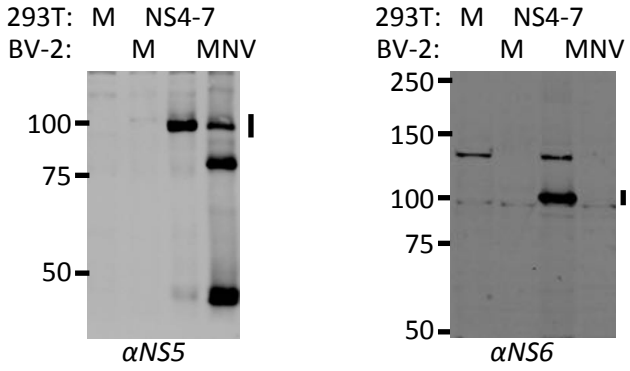

H) NS3-6

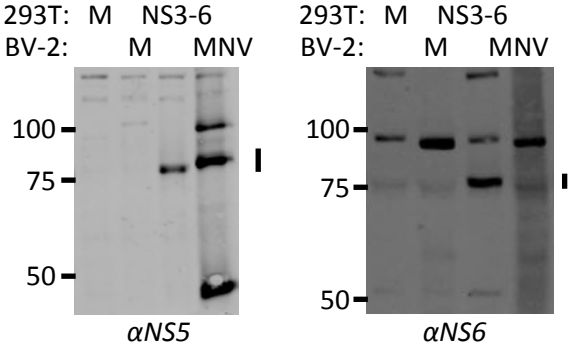

I) NS3-7

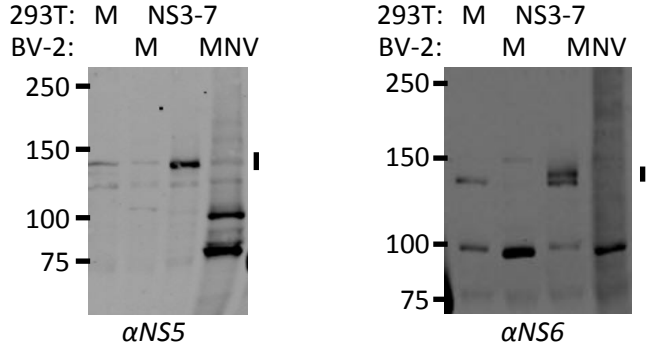

J) NS1/2-6

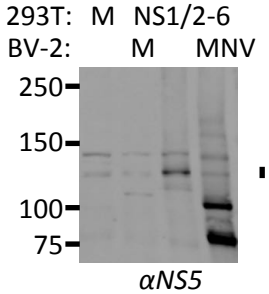

K) NS1/2-7

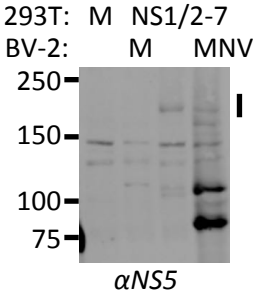

Fig S2.

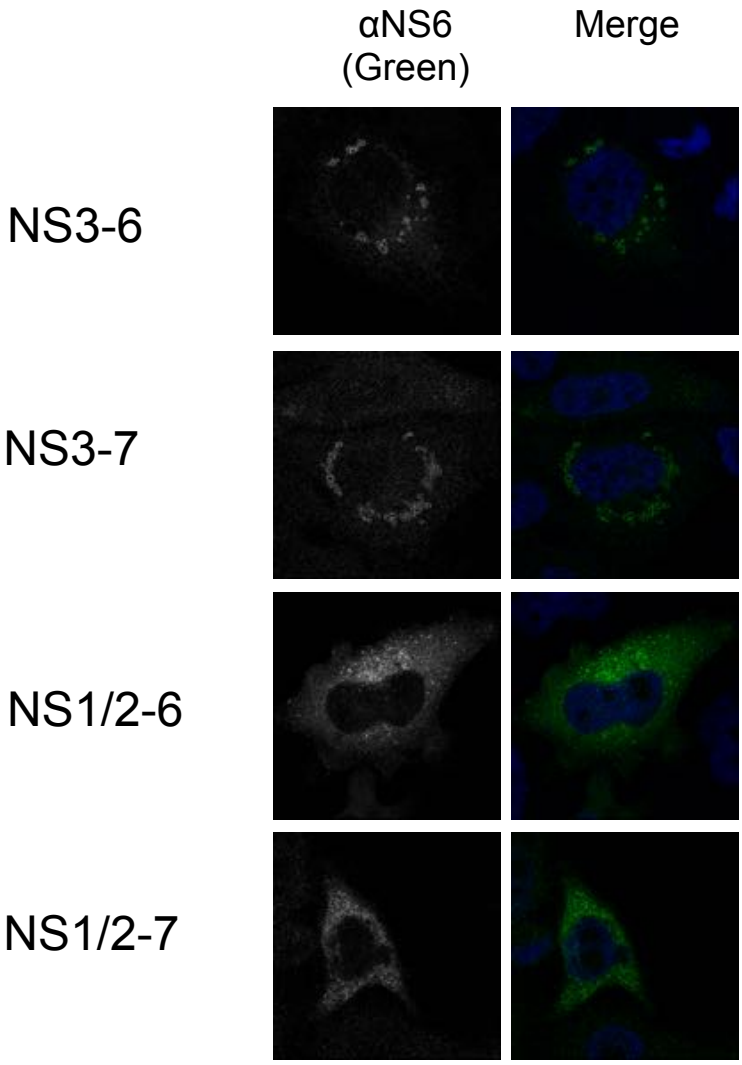

Fig S3.

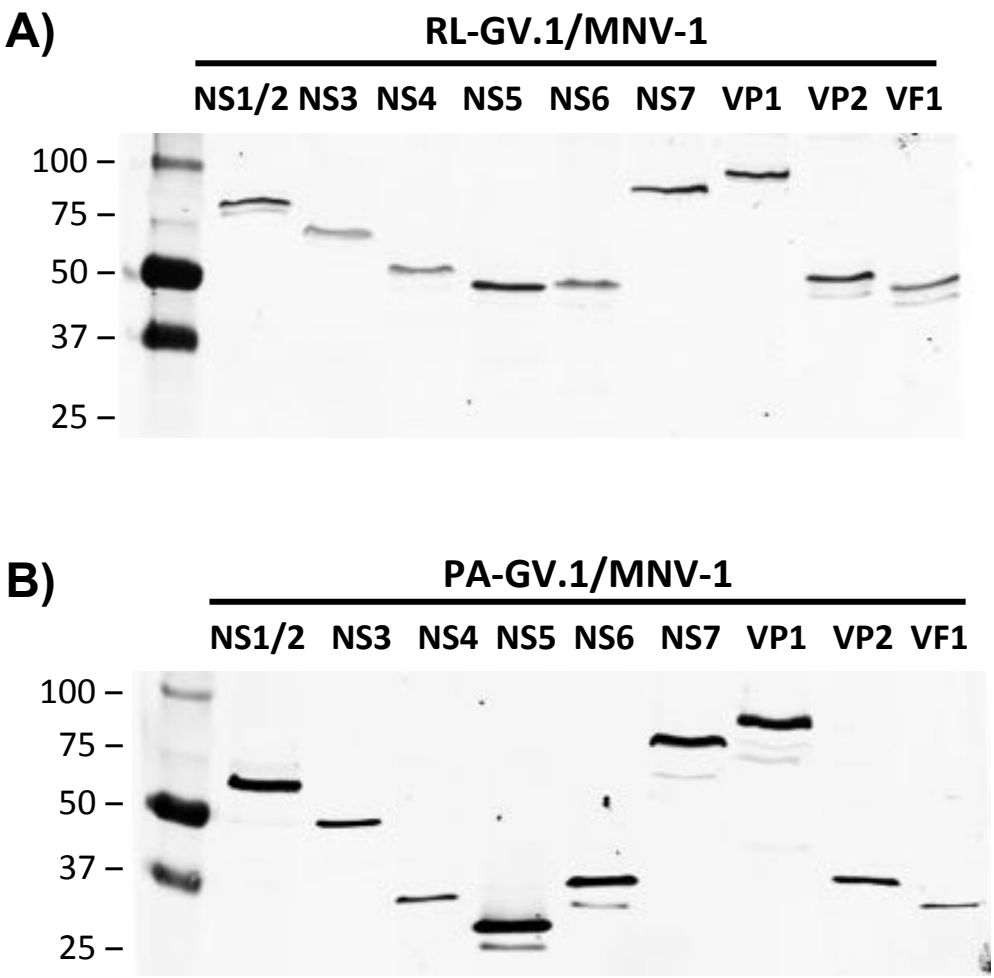
A)
RL-GV.1/MNV-1
NS1/2 NS3 NS4 NS5 NS6 NS7 VP1 VP2 VF1
100 –
75 –
50 –
37 –
25 –
B)
PA-GV.1/MNV-1
NS1/2 NS3 NS4 NS5 NS6 NS7 VP1 VP2 VF1
100 –
75 –
50 –
37 –
25 –

Fig S4.

A)

NV GI.1	Protein A fusion proteins							
Renilla luciferase fusion proteins	NS1/2	NS3	NS4	NS5	NS6	NS7	VP1	VP2
NS1/2	29.5	-0.9	21.5	0.6	1.7	4.1	0.3	-2.0
NS3	1.5	1.6	1.9	-0.4	0.3	0.1	-0.7	-0.7
NS4	37.7	-0.4	5.5	0.1	-3.2	-0.8	2.1	-2.5
NS5	-1.6	0.2	-0.6	1.3	1.6	11.5	0.6	-1.0
NS6	1.3	-2.4	-1.7	-2.1	-2.0	-2.3	0.0	-2.3
NS7	4.7	-1.3	-1.2	4.3	0.4	6.5	6.5	2.0
VP1	3.9	-0.1	2.0	1.5	-0.1	4.7	32.4	4.6
VP2	1.6	-0.7	-0.5	1.7	2.8	1.8	17.9	13.8

RZ-score scale	<3	3-6	6-9	9-12	12-15	>15

B)

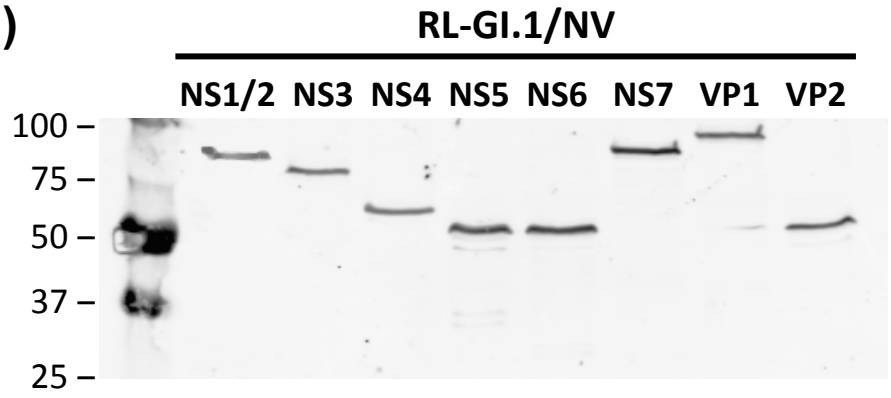

C)

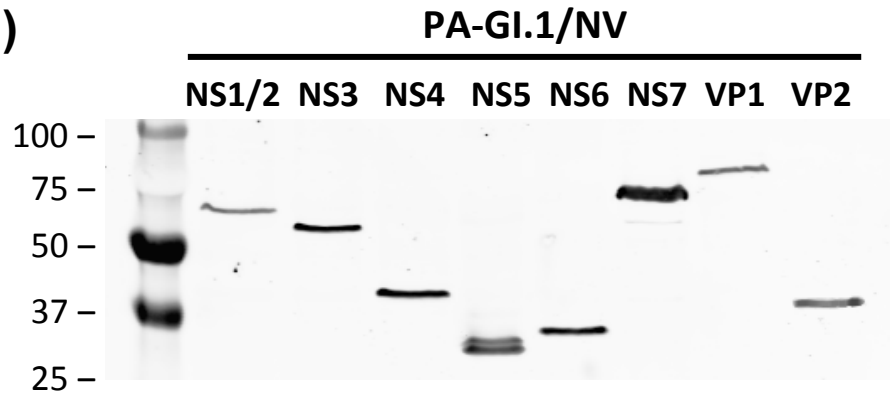

Fig S5.

A)

MD GII.4	Protein A fusion proteins: NS1/2	NS3	NS4	NS5	NS6	NS7	VP1	VP2
Renilla luciferase fusion proteins: NS1/2	27.3	1.6	27.8	0.8	1.2	3.2	1.4	1.5
NS3	1.1	1.0	-0.3	0.7	-0.1	0.3	0.0	0.0
NS4	24.9	-0.6	3.5	1.6	0.6	0.4	1.5	1.1
NS5	2.3	-0.3	-2.7	-0.6	-0.7	7.7	0.7	1.5
NS6	1.5	-1.2	-0.6	-0.6	0.8	-0.5	-0.9	-0.2
NS7	8.9	1.6	2.2	3.2	0.8	7.1	13.3	-1.8
VP1	5.9	-0.1	-0.7	2.3	0.6	5.4	8.6	13.9
VP2	2.0	1.3	-1.4	1.2	1.0	0.9	10.0	10.3

RZ-score scale	<3	3-6	6-9	9-12	12-15	>15

B)

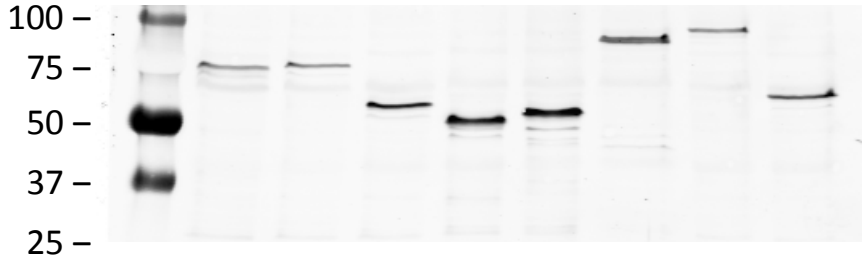

C)